



Geochemical signature of porphyries in the Baogutu porphyry copper belt, western Junggar, NW China

Ping Shen ^{*}, Yuanchao Shen, Tiebing Liu, Lei Meng, Huawu Dai, Yueheng Yang

Key Laboratory of Mineral Resources, Institute of Geology & Geophysics, Chinese Academy of Sciences, P.O. Box 9825, Beijing 100029, People's Republic of China

ARTICLE INFO

Article history:

Received 9 December 2008
Received in revised form 21 March 2009
Accepted 8 April 2009
Available online 17 April 2009

Keywords:

Ore-bearing porphyry
Geochemistry
Sr–Nd isotopes
Baogutu porphyry copper belt
Darbut arc
Western Junggar

ABSTRACT

The Baogutu porphyry copper belt lies in the Darbut transitional island arc of the western Junggar, in the western section of the Central Asian Orogenic Belt in NW China. Our new petrographic results for the ore-bearing porphyry stocks in the Baogutu porphyry copper belt recognize them as diorite porphyry stocks rather than the granodiorite porphyry stocks as previously identified. The copper mineralization is hosted in the diorite, diorite porphyries and related breccias of the diorite porphyry stocks.

Geochemical data indicate that the ore-bearing porphyries have a predominantly intermediate composition with a transitional character from tholeiite to calc-alkaline, and are enriched in large ion lithophile elements (LILE) and depleted in high field strength elements (HFSE) with a clear negative Nb anomaly. REE patterns show distinct enrichments in LREE relative to HREE. The rocks also exhibit high initial $\epsilon_{\text{Nd}}(t)$ (+2.7 to +6.3) ratios and low initial $^{87}\text{Sr}/^{86}\text{Sr}$ values (0.70359–0.70397). Many samples are chemically similar to adakites (e.g. $\text{Yb} < 1.9$ ppm, $\text{Y} < 18$ ppm, $\text{Sr}/\text{Yb} > 20$, $^{87}\text{Sr}/^{86}\text{Sr} < 0.7045$). These data are consistent with a transitional island arc from immature arc to mature arc and suggest that the ore-bearing porphyry system was derived from the partial melting of multiple sources including oceanic crust and a subduction-modified mantle wedge, with melts undergoing significant crystal fractionation during convergence between the paleo-Junggar ocean and the Darbut arc.

© 2009 International Association for Gondwana Research. Published by Elsevier B.V. All rights reserved.

1. Introduction

The Junggar terrane is an important section of the Central Asian Paleozoic accretionary and collisional orogenic belt between the Siberian and Tarim plates (Xiao et al., 2001; Qin et al., 2002; Safonova et al., 2002; Buslov et al., 2004; Xiao et al., 2008; see also Chai et al., 2009–this issue; Zhang et al., 2009–this issue, Zhao et al., 2009–this issue). Two early Carboniferous volcanic belts in the western Junggar, the Anqi volcanic belt and the Darbut volcanic belt, were first identified by Shen and Jin (1993). The two belts, separated by the Anqi fault, extend north-eastward from Liushugou in south-west, to Sertuohai in north-east, a distance of approximately 150 km (Figs. 1, 2). The Anqi volcanic belt is limited by the Anqi fault and the Hatu fault, and the Darbut volcanic belt is widespread over both sides of the Darbut fault/suture (Figs. 1, 2, Shen and Jin, 1993). Late Carboniferous to Permian granitic intrusions are widespread throughout the western Junggar (Jahn et al., 2000; Chen and Jahn, 2004; Chen and Arakawa, 2005). Gold and copper mineralization is well developed in volcanic rocks and

intrusions of the two volcanic belts, forming the Hatu gold metallogenic belt and the Baogutu copper metallogenic belt, respectively, separated by the Darbut fault/suture (Figs. 1, 2).

To the north of the Darbut fault, gold mineralization accompanying an early Carboniferous tholeiite (328 ± 31 Ma, Shen and Jin, 1993) is of great economic interest. About 200 gold deposits and occurrences of different sizes are clustered in a 100-km-long by 40-km wide corridor, forming the Hatu gold metallogenic belt (Shen et al., 1993, 1996).

To the south of the Darbut fault, many intermediate-acidic stocks have intruded into the Darbut volcanic belt. More than 20 ore-bearing stocks (named as stock I, II, III, IV, V, and so on), located mainly in the Baogutu area in the south of the Darbut fault, were discovered by Institute of Geology and Geophysics, Chinese Academy of Sciences in 1985–1990. Gold mineralization has been identified around these stocks which have been named as small-intrusion-related gold deposits by Shen Yuanchao (Shen et al., 1993, 1996). The disseminated copper mineralization in these stocks, especially in the stock II and V, has also been discovered at surface (Shen et al., 1993). Subsequently, four diamond drill holes completed in stock V by Institute of Geology and Geophysics, Chinese Academy of Sciences, one of them (ZK2801) totalling 354 m did encounter copper mineralization ($> 0.1\%$ Cu about 30 m in thick).

In 2002–2008, 52 diamond drill holes totalling 24,000 m have been completed by Institute of Geology, Xinjiang Geoexploration Bureau for Non-ferrous Metal in stock V. Disseminated and network copper-

^{*} Corresponding author. Tel.: +86 10 82998189; fax: +86 10 62010846.
E-mail address: pshen@mail.iggcas.ac.cn (P. Shen).

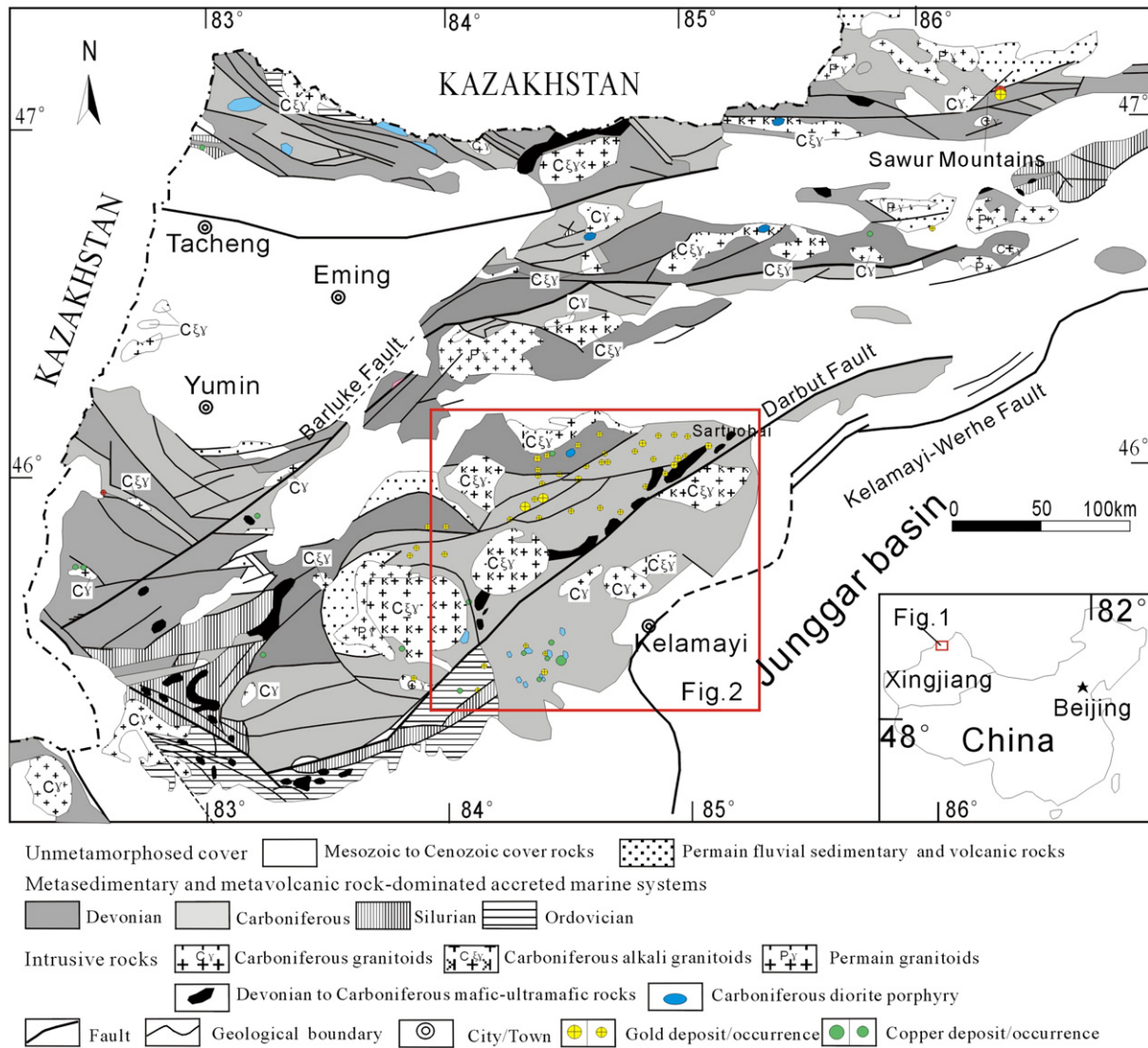


Fig. 1. Generalized geological map of the western Junggar, NW China, showing the distribution of the volcanic rocks, intrusions, and ophiolite belts (after Shen and Jin, 1993; Xiao et al., 2001; Qin et al., 2002; Xiao et al., 2008).

molybdenum–gold mineralization have been discovered which has been named as a porphyry copper deposit (Zhang et al., 2005, 2006c). A preliminary evaluation in 2006 showed that stock V contained an in situ resource of 111 tons averaging 0.28% Cu, >0.01% Mo, 0.25 ppm Au, and 2.8 ppm Ag. Based on these figures, stock V is Xinjiang's second largest porphyry copper deposit (the largest is the Tuwu–Yandong located in the eastern Tianshan, NW China). This and other porphyry occurrences, such as the stock I, II, III, IV, and VIII, form the Baogutu copper metallogenic belt (Figs. 2, 3). Due to a lack of water and infrastructure in the area, open pit mining has not yet been initiated, but is planned for the near future.

This paper addresses some unresolved questions on the petrology and petrogenesis of these ore-bearing porphyry stocks in the Baogutu copper belt. It has important implications for metallogenic prognosis and exploration programs in the Baogutu copper belt itself and, by inference, throughout the western Junggar. In addition, this information is also important for understanding the tectonic evolution and copper mineralization in western Junggar and even the Central Asian Orogenic Belt. Petrographic studies were carried out on 1024 thin sections of the rocks; thirty-two of them were selected for major and trace element analyses; fifteen whole-rock samples were analyzed for Sr and Nd isotopes.

2. Geological outline

The western Junggar, located between the Altay Shan and Tianshan, extends westward to the Junggar–Balkhash in adjacent Kazakhstan and eastward to the Junggar Basin in China (Fig. 1, Shen et al., 1996; Xiao et al., 2004). The western Junggar is characterized by Devonian to Lower Carboniferous metasedimentary rocks, andesites, basalts, and some melanges (Shen and Jin, 1993). Devonian volcanic rocks are distributed principally in the northwestern part of Junggar. Lower Carboniferous volcanic rocks are widespread throughout the southeastern part of Junggar, near the Darbut fault which formed the two important early Carboniferous volcanic belts of the western Junggar mentioned-above (Figs. 1, 2).

Although the two volcanic belts have similar rock assemblages which consist of volcanic, volcanoclastic and sedimentary sequences, the volcanic rocks in the Anqi volcanic belt contain tholeiites (quartz tholeiite and olivine tholeiite), an oceanic basalt assemblage, which suggests that they were erupted in an extensional back-arc basin setting based on an island arc background (Shen and Jin, 1993), while the volcanic rocks in the Darbut volcanic belt consist of a tholeiitic assemblage (quartz tholeiite and olivine tholeiite) and a calc-alkaline assemblage (andesitic basalt, trachybasalt, basaltic trachyandesite),

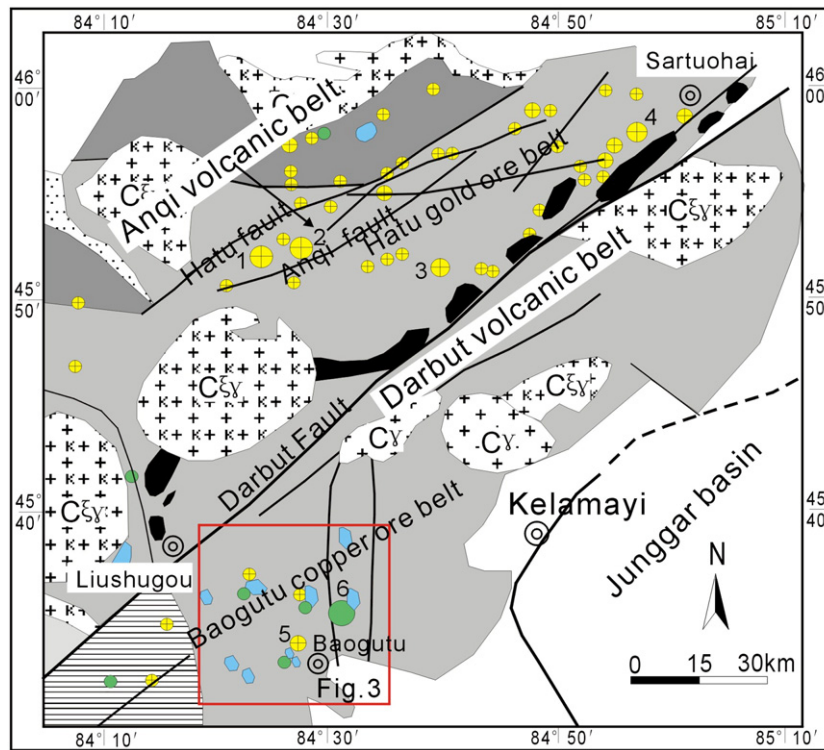


Fig. 2. Regional geological map of the Baogutu porphyry copper belt and the Hatu gold belt in the western Junggar showing the distribution of the Anqi volcanic belt and the Darbut volcanic belt and the location of the most important gold deposits and porphyry copper deposits. The northeast-trending Anqi fault separates the Anqi volcanic belt and the Darbut volcanic belt and the Darbut fault separates the Hatu gold belt and the Baogutu copper belt. Generalized after Shen et al. (1993), Shen and Jin (1993). Symbols are the same as in Fig. 1. Number and name of selected deposits: 1 – Hatu gold deposit (also called Qiqiu-1); 2 – Qiqiu-2 gold deposit; 3 – Baobei gold deposit; 4 – Sartuohai gold deposit; 5 – Baogutu gold deposit; 6 – Baogutu Cu–Mo deposit.

indicating a transitional island arc setting from back-arc basin to island arc (Shen and Jin, 1993) where the Baogutu copper ore belt is located.

Late Carboniferous to Permian magmatism is widespread throughout the western Junggar and is granitic in character (Chen and Jahn, 2004; Chen and Arakawa, 2005; Wang and Xu, 2006) and can be divided into two groups (Fig. 2, Shen and Jin, 1993; Hu et al., 1997). One is the barren granite batholiths which intruded into the Devonian to Lower Carboniferous volcanic rocks and were dominated by ~300 Ma (Hu et al., 1997; Su et al., 2006; Han et al., 2006) syenites and alkali granite. They represent production of juvenile continental crust in the Phanerozoic, triggered by upwelling of asthenosphere in an extensional regime (Chen and Arakawa, 2005). The other group is comprised of productive intermediate-acidic stocks which intruded into the Carboniferous Darbut volcanic belt and were dominated by 322–305 Ma by quartz diorite and granodiorite (Shen and Jin, 1993). The ore-bearing intrusions in the Baogutu copper belt belong to the latter (Shen et al., 2008).

Geological and petrographic descriptions from the two volcanic belts in the western Junggar were reported by Shen and Jin (1993). Three Early Carboniferous stratigraphic units have been identified that are older than the ore-bearing porphyry stocks: Tailegula Group, Baogutu Group, and Xibeikulasi Group from the bottom up. The ages of Tailegula Group rocks are determined. The pillow basalt and chert in the Anqi volcanic belt yielded Rb–Sr ages of 328 ± 31 Ma (Shen et al., 1993; Li and Chen, 2004) and 323 ± 22 Ma (Li and Chen, 2004), respectively. The tuff in the Darbut volcanic belt has a U–Pb zircon SHRIMP age of 328.1 ± 1.8 Ma (Wang and Zhu, 2007).

The main structures of the western Junggar are characterized by a series of approximately ENE-trending faults, including the Darbut fault/suture, and the Mayile and Barluke faults (Fig. 1). Of these, the Darbut fault/suture is the most important because it was the locus of intense magmatism and associated mineralization. The lithologies, folds and major faults trend NS in the south of the Darbut fault,

especially in the Baogutu area, and are almost orthogonal to those of the north of the Darbut fault (Figs. 2, 3).

3. Ore-bearing porphyries and mineralization

More than 20 porphyry stocks are distributed in the Darbut volcanic belt, of these the stock I, II, III, IV, and VIII, located in the Baogutu copper belt, are ore-bearing porphyries (Fig. 3). They were intruded into volcanic, volcanoclastic and sedimentary sequences of the Early Carboniferous Tailegula Group, Baogutu Group, and Xibeikulasi Group (Fig. 3). They are mostly irregular in shape at the surface, with different sizes, the largest (stock I) is 4 km^2 in areas and the secondary body is stock II with a 3 km^2 area, all other bodies are $< 1 \text{ km}^2$.

We observed and logged the drill cores and outcrops of stocks I, II, III, IV, and VIII. Petrographic studies were carried out on 1024 thin sections of samples selected from drill cores and surface exposures. As a result, we identified these ore-bearing porphyry intrusions as dioritic porphyritic stocks. This is also strongly supported by the alteration characteristics and the geochemistry of the 32 ore-bearing porphyry samples (discussed below in detail). This is in disagreement with earlier results that the ore-bearing porphyries are granodiorite porphyries (Zhang et al., 2005, 2006a,c; Cheng and Zhang, 2006; Song et al., 2007).

Almost all ore-bearing porphyry stocks have the same rock assemblage: diorite/quartz diorite, diorite porphyry/quartz diorite porphyry, related breccias, and minor granodiorite porphyry. The ore-bearing porphyry stocks also have the same disseminated and network Cu–Mo–Au mineralization as the Cu–Mo mineralization developed within the ore-bearing stocks. Cu–Au mineralization occurred in the upper stocks and the contact zone between the stocks and wall rocks, while single Au mineralization occurred in the outer wall rocks. The mineralization is associated mainly with diorite porphyries/quartz

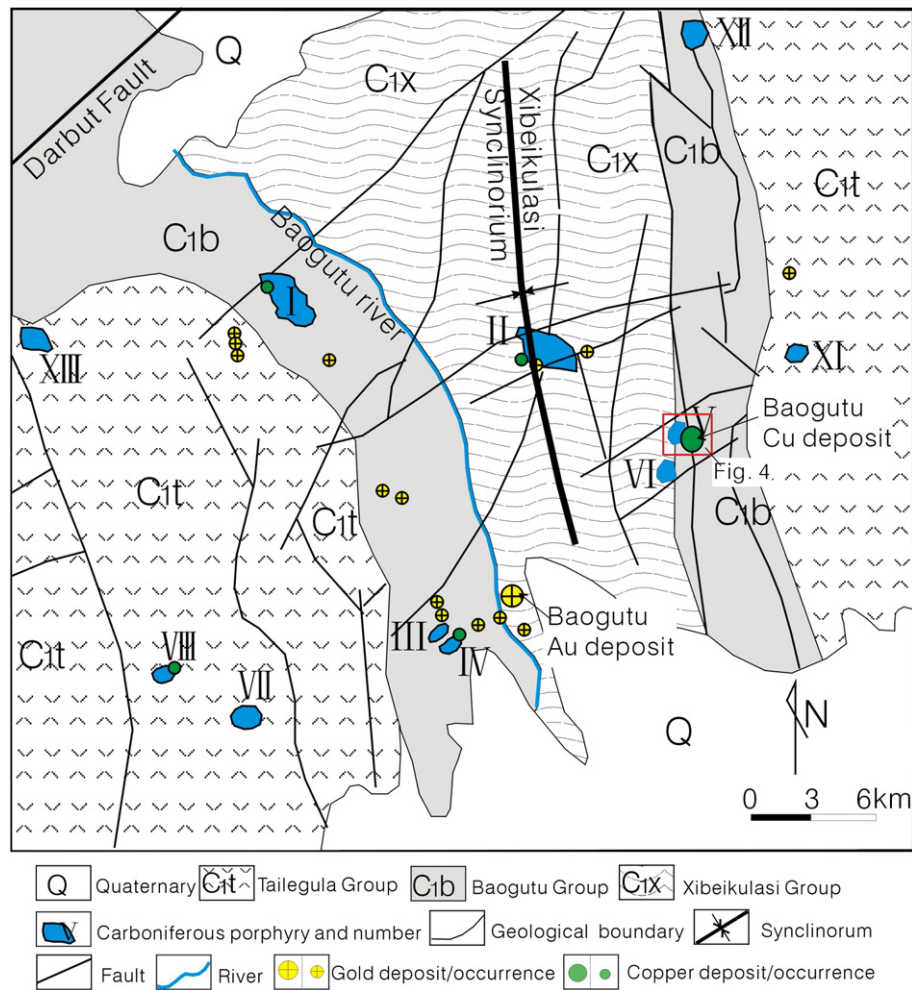


Fig. 3. Geological map of the Baogutu porphyry copper belt in the western Junggar (after Shen and Jin, 1993).

diorite porphyries, diorite/quartz diorite, and related breccias rather than the granodiorite porphyry previously identified. Stock V is the most important ore-bearing porphyry in the Baogutu copper belt. The other ore-bearing porphyry stocks are distributed around stock V and located from 5 km to 20 km to the east of stock V (Fig. 3), and have similar features to those of stock V. Stock V, therefore, is used here as an example for detailing the geology and petrography of the ore-bearing intrusions.

3.1. Ore-bearing porphyries

Stock V has a plan area of approximately 0.84 km² and is intruded along the east limb of the Xibeikulasi syncline into silty tuff and tuffaceous siltstone of the Baogutu Group and siltstone and tuffaceous stone of the Xibeikulasi Group (Fig. 4).

We document the geological and petrographic characteristics of stock V based on our research of 686 thin sections of the drill cores and outcrops, observations from more than 24,000 m of drill core, and logs of 13 drill holes (Fig. 4, ZK107, 105, 111, 103, 109, 101, 102, 106, 603, 403, 203, 303, 503, 211, 009). The locations of the part samples are shown in Figs. 4, 5. New results for stock V identify the intrusion as a dioritic porphyritic stock which contains diorite, diorite porphyry/quartz diorite porphyry, related later breccias, and minor granodiorite porphyry. The diorite and predominant diorite porphyry/quartz diorite porphyry is distributed from centre outwards (Figs. 4, 5). The breccias occurred within and adjacent to the ore-bearing intrusion and overprinted the earlier other two rock types (diorite and diorite

porphyry) and wall-rocks (Fig. 5). Almost all rocks are fine- to medium-grained (1–3 mm) and contain the same assemblage of minerals: plagioclase, pyroxene, hornblende, biotite, quartz, minor titanite, rutile, apatite, magnetite, and zircon.

Diorite is granular, and ranges from fine-medium- (1–2 mm) to medium-coarse-grained (2–3 mm) and occurs at depths of 420 m to at least –640 m below the present erosional surface (Fig. 5). The gradual contact with the diorite porphyry/quartz-diorite porphyry is commonly brecciated (Fig. 5). According to the dominant dark mineral, diorite comprises hornblende diorite (Fig. 6A) and biotite (quartz) diorite. Biotite (quartz) diorite (<30% by volume) is subordinate to hornblende diorite. Almost all diorites contain the same assemblage of minerals: plagioclase (50–60 vol.%), quartz (5–15 vol.%), brown hornblende (15–20 vol.%), brown biotite (5–10 vol.%), pyroxene (<5% vol.%), minor titanite, rutile, apatite, magnetite, and zircon. Plagioclase generally is complexly zoned, twinned andesine (An_{37–50}) and labradorite (An_{50–58}). Hornblende diorite contains minor quartz (<5% by volume), while biotite diorite has more quartz, but generally less than 10–15% by volume.

The diorite porphyry/quartz-diorite porphyry units are found around the outer edge of the diorite (Fig. 5). The contact between diorite porphyry/quartz-diorite porphyry and early Carboniferous tuff, tuffaceous stone, and siltstone is exposed in the northern part of the study area.

The diorite porphyry/quartz diorite porphyry units closely resemble diorite in their mineralogy and comprise hornblende diorite porphyry (Fig. 6D) and biotite quartz diorite porphyry (Fig. 6B). All

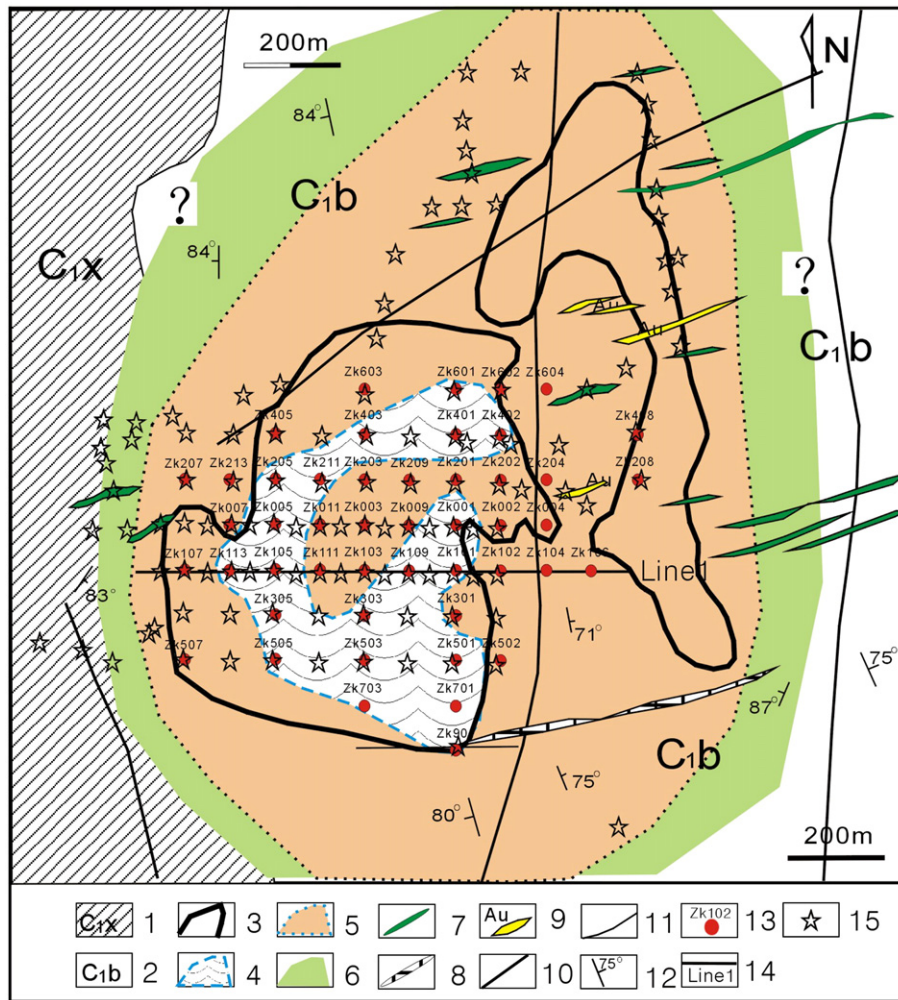


Fig. 4. Geological map of the Baogutu porphyry Cu–Mo deposit showing the porphyry intrusion after Shen and Jin (1993); inferred extensions of the alteration type performed by authors. Beeline (line 1) shows location of the geological exploration section, dots indicate the position of drill holes, and pentagons show the location of the samples for this study. 1 – tuffaceous siltstone, and siltstone of the Xibeikulasi Group; 2 – tuff and tuffaceous siltstone of the Baogutu Group; 3 – diorite porphyry; 4 – phyllic alteration zone; 5 – potassic zone; 6 – propylitic zone; 7 – diorite and diabase dikes; 8 – granite dike; 9 – gold orebody; 10 – fault; 11 – boundary of geology; 12 – stratigraphic occurrence; 13 – location of boreholes and number; 14 – location of the geological exploration section and number; 15 – location of samples.

contain about 20–30% phenocrysts of plagioclase, hornblende, biotite in a matrix dominated by plagioclase and hornblende. According to the grain-size of the matrix, we described a group of mainly medium-grained porphyries and one of minor fine-grained porphyry in this stock. The fine-grained porphyry is distributed around the predominant medium-grained porphyry (Fig. 5).

The matrix in the medium-grained porphyry is 0.1–0.5 mm in grain size and generally makes up 60–70 vol.% of the rocks (Fig. 6B–D). Phenocrysts in medium-grained porphyry comprise about 30–40 vol.% of the rock and are up to 2–3 mm in diameter including plagioclase (15–20 vol.%), hornblende (10 vol.%), biotite (5 vol.%), and pyroxene (<3 vol.%). Fine-grained porphyry consists of clear phenocrysts and matrix grain-size ranges, similar to volcanic rock (Fig. 6E) but with hornblende occurring in the matrix. The phenocrysts of plagioclase, hornblende and biotite have grain sizes of 2–3 mm and account for 10–15 vol.% of the rock, while the matrix is microcrystalline plagioclase, hornblende, and minor quartz occupy 85–90 vol.% of the rocks.

Two major breccias have been identified on the basis of clast lithology and composition of the breccia matrix. The clast-supported breccias with sandy matrix are ore-bearing and formed by a final phase of magmatic hydrothermal activity. The hydrothermal breccias with an abundant chalcopyrite–pyrite overprint are fissure-supported

breccias with hydrothermal mineral matrix (Fig. 6F, H). A feature of the breccias is that it contains predominant ore bodies (Fig. 5).

3.2. Alteration and mineralization

The alteration characteristics of the ore-bearing porphyry confirm the petrography results discussed above. Rocks in the studied stock V area were subjected to intense hydrothermal alteration, especially within and adjacent to the ore-bearing intrusion. Petrographically, fresh rocks were only available for sampling at depths 500 m below the present erosional surface. Even in the outermost part of the area, it is impossible to find completely fresh rocks in outcrop. Except at depth, pyroxene has been replaced by hornblende (Fig. 6C) and is recognizable from the characteristic pyroxene morphology of pseudomorphs. Hornblende has also been partly or completely replaced by biotite and magnetite (Fig. 6D). The biotite has been replaced by secondary biotite, and in some cases rutile needles aligned in the direction of the principal cleavages. Plagioclase has been partly or completely replaced by sericite (Fig. 6D).

We document the alteration characteristics of stock V based on our research of 170 thin sections of the outcrops, with the locations of the samples in Fig. 4. This stock is characterized by a widespread

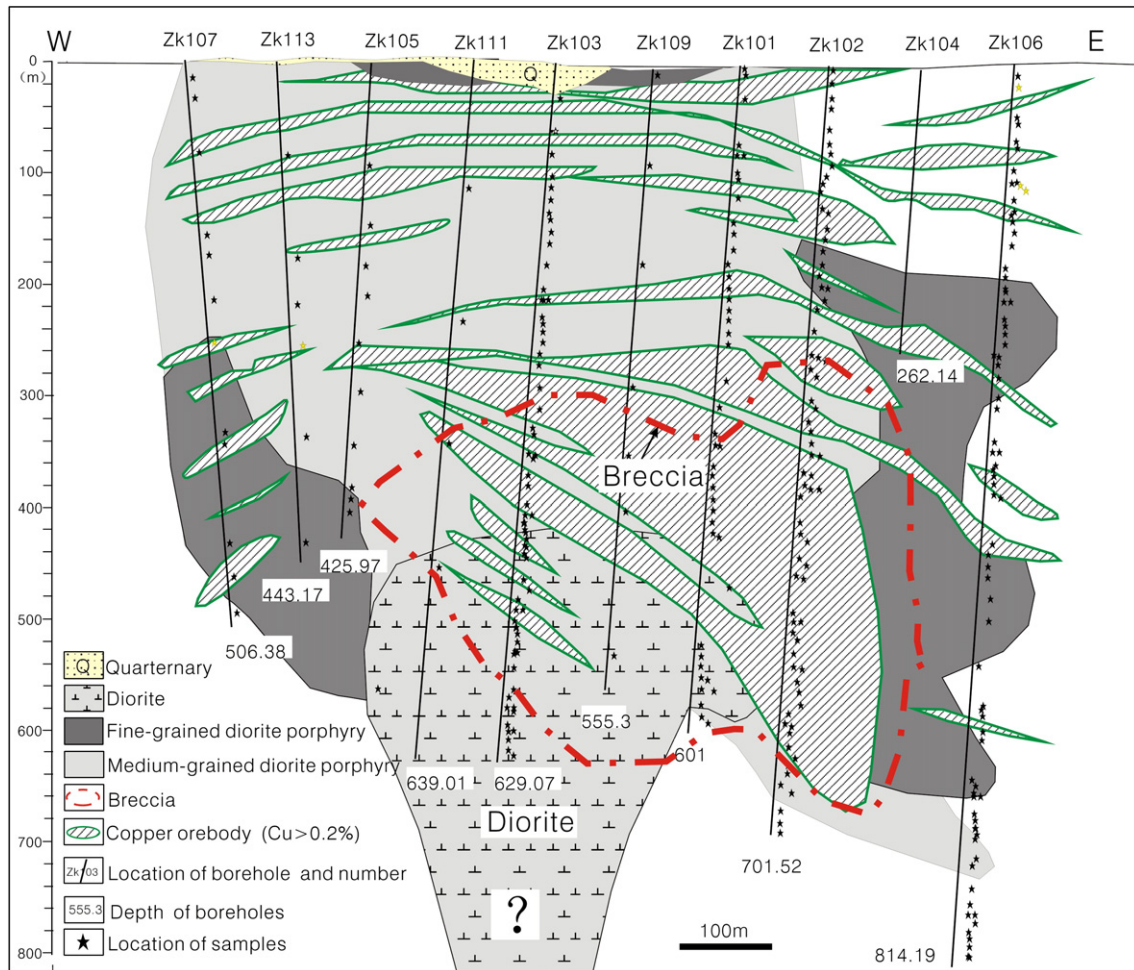


Fig. 5. Cross section along section Line 1 with lithologies across Bagutu porphyry Cu–Mo deposit (measured by authors) showing the copper ore bodies (after Zhang et al., 2006c). See Fig. 4 for location. Symbols are the same as in Fig. 4.

potassic alteration that is defined by the assemblage biotite–quartz–(magnetite–chlorite). It is remarkable that K-feldspar is rare in the potassic zone of the stock and the main ore zones are closely associated with biotite in the potassic zone. The potassic zone is overprinted by the limited phyllic alteration zone where the sericite–quartz assemblage is more abundant but biotite is also present. In the outer zone biotite disappears and the propylitic alteration assemblage epidote–chlorite–calcite is present. A well-defined argillic zone does not occur in this stock. Argillic alteration is limited to veinlets and partly replaces plagioclase phenocrysts. The phyllic alteration is limited to the inner parts of the potassic zone rather than a well-defined phyllic ring. All these characteristics indicate that the Baogutu stock V system corresponds to a diorite-type porphyry copper model (Hollister et al., 1974; Barthelmy, 1979) rather than the classic type or granodiorite-type porphyry copper (Lowell and Guilber, 1970; Tittle and Beane, 1981). This supported our suggestion that the ore-bearing porphyries in the Baogutu copper belt are diorite porphyries rather than the classic granodiorite porphyries.

The ore bodies extend over 600 m below the surface (Fig. 5) within the stock, minor occurrences are found in the wall rocks. The ore occurs essentially in disseminations, veins, veinlets, and breccias (Fig. 6G–I) that occupy the whole of the stock and limited wall rocks (Fig. 5). The breccias (Figs. 5, 6H) contain the important mineralization types, and overprint the early disseminated and veinlet ores where the dominant ore bodies occur. As well as these, two main types of veins are

distinguished: (1) quartz–chalcopyrite–pyrite veins (Fig. 6I) and (2) quartz–chalcopyrite–molybdenite veins (Fig. 6G).

The ages of stock V in the Baogutu copper belt are 322 ± 30 Ma (Shen et al., 1993). We obtained a U–Pb zircon SHRIMP age of 325.1 ± 4.2 Ma (unpublished data). The molybdenites from several veins of stock V have been dated by the Re–Os method, and yielded an age of 310 Ma (Song et al., 2007).

4. Geochemistry and isotope geochemistry

Samples used in this paper were collected from the ore-hosting porphyries I, II, III, IV, V, and VIII in the Baogutu copper belt. Most of the samples come from drill cores, and partly from outcrops. In addition to these samples, one outcrop of wall-rock (silty tuff) in the Baogutu copper belt was also analyzed (Table 1) for comparison.

Owing to relatively extensive alteration in these districts, the porphyries were more or less all affected by silicification, biotitization, and sericitization. The least altered samples were chosen for major element, trace element, and Sr–Nd isotope analyses. Results are listed in Tables 1 and 2. Analyses were performed at the Institute of Geology and Geophysics, Chinese Academy of Sciences.

Major elements were analyzed by XRF-1500 Sequential X-ray Fluorescence Spectrometry, with wet chemical determination of FeO and loss-on-ignition (LOI). Analytical precision based on certified standards and duplicate analyses are expressed in terms of relative percentages, which range from $\pm 0.01\%$ to $\pm 0.20\%$. A PQ2 Turbo

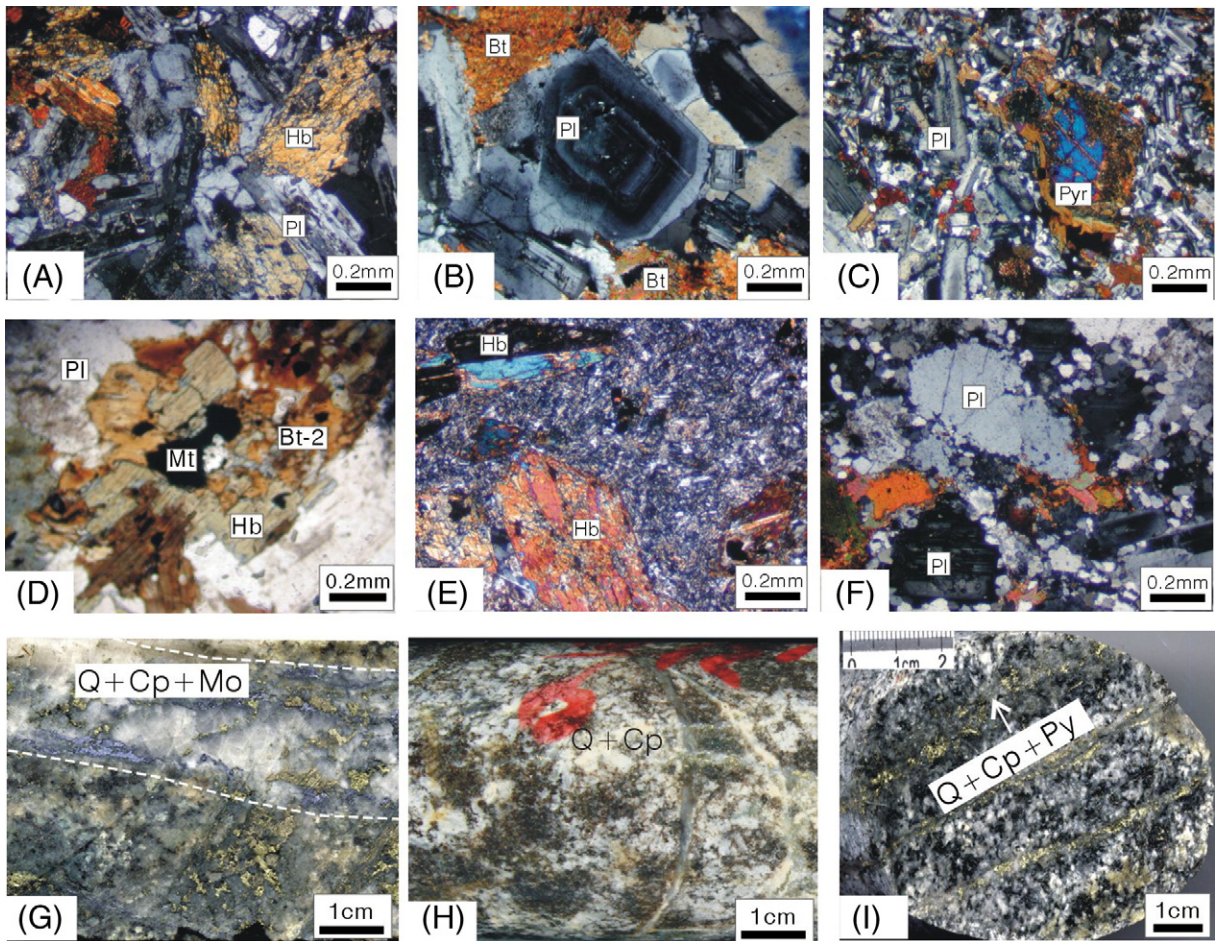


Fig. 6. Photomicrographs of the dioritic porphyritic stock and ores. (A) – hornblende diorite with plagioclase, hornblende, minor biotite, and rare magnetite; (B) – medium-grained biotite diorite porphyry, phenocrysts of plagioclase, biotite set in a fine-grained matrix consisting mainly of plagioclase, biotite and minor quartz; the plagioclase phenocrysts are andesine in the form of zoned and twinned crystals. (C) – medium-grained pyroxene diorite porphyry, phenocrysts of plagioclase and pyroxene set in a fine-grained matrix consisting mainly of plagioclase and hornblende; (D) – medium-grained hornblende diorite porphyry, hornblende has also been partly replaced by biotite and magnetite; (E) – fine-grained hornblende diorite porphyry, phenocrysts of hornblende and plagioclase set in a microcrystalline matrix consisting of plagioclase and hornblende; (F) – ore-bearing hydrothermal breccia with hydrothermal mineral matrix consisting of biotite, quartz, and sulfides; (G) – ore with quartz–chalcopyrite–molybdenite veins; (H) – ore-bearing hydrothermal breccia; (I) – ore with quartz–chalcopyrite–pyrite veins. Abbreviations: Pyr: pyroxene; Hb: hornblende; Bt: biotite; Bt-2: secondary biotite; Mt: magnetite; Pl: plagioclase; Q: quartz; Py: pyrite; Cp: chalcopyrite; Mo: molybdenite.

inductively Coupled Plasma Mass Spectrometer (ICP-MS) was used to analyze trace elements and REE. One hundred grams of sample was digested in beakers using a hot HF + HNO₃ mixture followed by a HF + HNO₃ + HClO₃ mixture to ensure complete dissolution and then taken up in 1% HNO₃ (dilution factor of ~500). The measurement error and drift were controlled by regular analysis of standard samples with a periodicity of 10%. Analyzed uncertainties of ICP-MS data at the ppm level are better than ±3%–±10% for trace elements, ±5%–±10% for REE (Table 1). Sr–Nd isotope compositions were determined on a MAT262 mass spectrometer. Details of the chemical procedures were described by Chen et al. (2002). Procedural blanks were <100 pg for Sm and Nd and <50 pg for Rb and Sr. Typical within-run precision (2σ) for Sr and Nd was estimated to be ±0.000010 and ±0.000013, respectively. The measured values for the JMC Nd standard and NBS987 Sr standard were ¹⁴³Nd/¹⁴⁴Nd = 0.511937 ± 7 (2σ, n = 12) and ⁸⁶Sr/⁸⁸Sr = 0.710226 ± 12 (2σ, n = 12), respectively, during the period of data acquisition (Table 2).

4.1. Major and trace elements

Fig. 7 shows two diagrams illustrating the most important chemical features of the rocks analyzed from the ore-bearing porphyries and wall-rock in the Baogutu copper belt. Although careful choices of samples in the field and microscopic investigations

have allowed the selection of suitable (least altered) samples for geochemical analysis, the influence of the hydrothermal alteration cannot be completely ruled out (Martins et al., 2009). Therefore we chose the Zr/TiO₂ versus Nb/Y diagram and Zr versus Y diagram for the chemical classification of the rocks (Fig. 7a, b). In the Zr/TiO₂ versus Nb/Y diagram (Fig. 7a), the samples from the ore-bearing porphyries plot mainly in the andesite/basalt to andesite fields. Tuff samples plot in the andesite field. This whole-rock chemistry supports our field observation and petrography research that the Baogutu ore-bearing porphyries have a predominantly intermediate, and minor felsic composition. Therefore, the porphyry stocks with SiO₂ contents ranging from 52% to 66% (Table 1) can be classified by their petrography and whole-rock chemistry as ranging mainly from diorite to quartz diorite, with minor granodiorite.

In the Zr versus Y diagram (Fig. 7b), almost all samples fall into the field of calc-alkaline and transitional volcanics as defined by Barrett and MacLean (1994) and show that these porphyry stocks have a transitional character from tholeiite to calc-alkaline. A volcanoclastic sample (silty tuff) has 57 wt.% SiO₂ and plots in transitional volcanics.

Mantle-normalized trace element patterns depict three rock suites with different magmatic histories (Fig. 8). Calc-alkaline quartz diorites in stocks I, II, and V (Fig. 8b, d, h) exhibit distinctly fractionated REE patterns and low HREE abundances. A second type of sample

Table 1
Major (wt.%) and trace element (ppm) abundance of representative porphyries in the Baogutu copper belt, the western Junggar.

Porphyry	I							II				
	BGT-1	NZK001-191	BGT-600	BGT-1700-1	ZK702-49	ZK702-166	ZK702-190	BGT-2	ZK007-85	ZK007-111	ZK007-124	
Sample	D	QD	D	D	QD	D	D	QD	QD	QD	QD	
Rock type	D	QD	D	D	QD	D	D	QD	QD	QD	QD	
SiO ₂	57.06	63.72	51.83	57.85	64.09	58.38	55.73	61.08	65.89	65.13	65.37	
TiO ₂	0.75	0.55	1.04	0.89	0.53	0.72	0.89	0.68	0.54	0.57	0.54	
Al ₂ O ₃	17.19	16.16	18.26	16.78	15.67	16.59	17.21	16.99	15.35	15.23	14.89	
Fe ₂ O ₃	3.57	1.72	2.37	2.56	1.70	2.06	2.60	2.99	1.37	1.65	1.05	
FeO	3.24	2.26	5.94	4.01	2.33	3.18	2.75	2.62	2.42	2.46	3.07	
MnO	0.09	0.05	0.13	0.11	0.06	0.06	0.05	0.04	0.04	0.05	0.04	
MgO	4.39	2.93	5.94	4.43	2.98	5.16	3.87	2.47	2.36	2.63	2.44	
CaO	6.17	4.78	8.32	6.38	4.54	6.06	6.24	2.01	3.89	4.02	3.70	
Na ₂ O	3.72	4.61	4	3.95	4.23	4.67	5.12	1.91	4.08	4.09	4.04	
K ₂ O	1.52	1.78	0.45	1.04	1.77	0.40	2.97	3.69	2.91	2.66	2.82	
P ₂ O ₅	0.16	0.14	0.21	0.21	0.13	0.16	0.29	0.21	0.12	0.13	0.12	
LOI	1.72	0.57	0.75	1.23	1.33	1.87	1.61	4.85	0.65	0.79	1.29	
Total	99.58	99.32	99.29	99.48	99.40	99.35	99.38	99.54	99.67	99.46	99.41	
Sc	15.65	8.89	24.89	16.22	9.57	14.87	16.77	13.85	8.73	9.71	9.22	
Cr	81.09	45.23	92.81	83.99	53.08	167.9	26.93	39.85	35.21	39.98	40.24	
Co	20.33	13.60	33.05	23.91	15.14	23.90	15.31	14.96	10.80	11.88	11.67	
Ni	37.1	30.37	76.08	54.56	33.97	111.0	35.08	23.2	21.09	26.61	19.75	
Cu	63.24	4.51	19.52	39.97	403.2	92.08	70.48	3344	96.47	49.05	50.03	
Zn	67.3	24.31	70.36	74.53	35.85	31.55	36.93	143.8	25.60	28.72	26.47	
Ga	20.64	18.16	21.55	19.15	18.66	21.62	22.62	18.75	18.70	18.13	17.65	
Rb	25.06	20.32	3.84	17.14	25.52	5.39	21.72	119.5	61.49	53.34	59.54	
Sr	881	747.4	830.5	626.5	636.1	921.9	908.7	165	459.2	496.8	446.4	
Y	10.7	7.98	17.81	16.26	8.73	7.47	11.89	14.89	15.03	14.93	14.24	
Zr	52.72	88.16	64.91	138.0	90.96	54.04	79.47	90.11	157.2	171.5	160.79	
Nb	1.6	2.08	2.16	3.35	2.46	1.13	2.40	3.98	3.81	3.86	3.80	
Mo	0.43	–	–	–	–	–	–	1.36	–	–	–	
Sn	0.67	–	–	–	–	–	–	1.32	–	–	–	
Cs	1.06	0.60	0.27	0.69	1.54	0.46	1.01	2.84	1.78	2.41	2.06	
Ba	696	608.3	285.4	422.0	573.7	273.0	542.5	491	716.5	708.9	692.5	
La	6.59	11.0	9.19	13.19	10.67	4.12	24.61	17.21	31.14	14.63	12.87	
Ce	16.13	20.95	21.12	26.76	20.56	9.25	55.16	31.05	57.39	29.42	25.96	
Pr	2.23	2.71	3.29	3.64	2.76	1.66	7.86	4.33	6.49	3.79	3.38	
Nd	10.35	10.97	14.50	15.01	10.50	7.41	31.86	18.83	23.13	14.80	13.34	
Sm	2.2	2.07	3.54	3.40	2.16	1.98	6.51	3.35	3.67	3.13	2.68	
Eu	0.97	0.73	1.14	1.04	0.71	0.64	1.9	1.17	0.88	0.83	0.73	
Gd	2.33	1.81	3.45	3.21	1.86	1.61	4.71	3.26	3.20	2.66	2.43	
Tb	0.36	0.26	0.55	0.49	0.28	0.24	0.53	0.49	0.47	0.42	0.37	
Dy	2.08	1.49	3.36	3.00	1.60	1.43	2.58	2.69	2.68	2.61	2.36	
Ho	0.43	0.28	0.69	0.62	0.31	0.27	0.46	0.57	0.54	0.54	0.48	
Er	1.13	0.76	1.91	1.72	0.86	0.72	1.14	1.54	1.55	1.51	1.39	
Tm	0.16	0.11	0.27	0.25	0.12	0.1	0.16	0.23	0.24	0.22	0.20	
Yb	1.11	0.70	1.75	1.65	0.82	0.62	1.02	1.44	1.60	1.44	1.33	
Lu	0.17	0.11	0.25	0.25	0.12	0.09	0.15	0.23	0.25	0.22	0.20	
Hf	1.79	2.61	1.91	3.93	2.72	1.72	2.36	2.81	4.73	5.00	4.72	
Ta	0.49	0.15	0.12	0.21	0.19	0.07	0.13	0.34	0.31	0.32	0.31	
Pb	3.11	2.85	2.19	4.62	3.11	1.84	1.90	3.25	4.58	4.50	4.49	
Bi	0.03	0.01	0.06	0.03	0.03	0.01	0.05	0.29	0.05	0.03	0.10	
Th	1.44	2.6	0.29	1.17	2.89	0.38	3.81	4.95	5.74	6.16	5.27	
U	0.43	0.73	0.13	0.37	1.06	0.49	3.56	2.55	1.32	1.45	1.67	
LREE/HREE	4.95	8.74	4.30	5.62	7.87	4.89	11.86	7.26	11.60	6.89	6.69	
ΣREE	46.29	54.03	65.06	74.28	53.40	30.21	138.70	86.45	133.3	76.29	67.79	
Porphyry	III					IV						
	BGT3-1	BGT3-3-1	BGT3-3-2	ZK01-1	ZK01-6	ZK2002-32	ZK2002-102	BGT-4-1	BGT-4-2	BGT4-1	BGT4-2	BGT4-3
Sample	D	D	D	D	D	D	D	D	D	D	D	D
Rock type	D	D	D	D	D	D	D	D	D	D	D	D
SiO ₂	53.76	52.38	53.19	60.42	58.45	57.97	59.13	58.18	58.61	57.38	58.91	57.35
TiO ₂	0.84	0.75	0.77	0.71	0.78	0.66	0.62	0.74	0.7	0.73	0.75	0.98
Al ₂ O ₃	18.7	16.47	17.35	17.45	17.39	15.70	16.94	17.66	17.28	16.98	16.59	16.37
Fe ₂ O ₃	2.87	2.49	2.98	1.54	1.17	1.59	1.13	2.39	1.78	2.54	2.03	3.17
FeO	4.36	4.90	4.63	4.07	4.97	4.9	4.15	4.14	4.64	4.74	4.58	4.28
MnO	0.14	0.11	0.12	0.09	0.11	0.10	0.10	0.09	0.09	0.11	0.09	0.09
MgO	4.56	6.03	5.98	2.88	3.63	3.89	3.94	3.21	3.37	4.3	3.56	3.85
CaO	7.53	7.89	8.69	5.98	6.33	4.35	4.90	6.28	5.54	6.73	5.85	6.43
Na ₂ O	3.77	3.26	3.04	4.18	4.03	5.02	5.26	4.07	3.98	3.96	3.85	3.69
K ₂ O	0.65	1.18	0.54	1.05	1.16	1.54	1.44	1.26	1.35	0.96	1.5	1.49
P ₂ O ₅	0.16	0.17	0.15	0.18	0.17	0.18	0.17	0.16	0.16	0.18	0.17	0.26
LOI	2.23	3.93	2.13	0.79	1.15	3.51	1.53	1.32	2.18	1	1.78	1.59
Total	99.57	99.56	99.57	99.39	99.39	99.45	99.36	99.5	99.68	99.61	99.66	99.55
Sc	17.19	19.91	22.75	11.69	16.72	14.03	11.62	15.39	14.91	15.93	16.13	16.75
Cr	45.82	156.4	141.0	15.59	16.71	79.49	79.29	43.04	40.58	115.77	70.24	56.54
Co	17.6	25.55	26.36	16.59	23.04	16.60	16.39	17.95	17.44	22.3	20.13	22.96
Ni	15.09	51.42	39.03	12.31	17.57	36.10	46.98	15.51	15.63	43.48	33.72	29.5

Table 1 (continued)

Porphyry	III					IV						
	BGT3-1	BGT3-3-1	BGT3-3-2	ZK01-1	ZK01-6	ZK2002-32	ZK2002-102	BGT-4-1	BGT-4-2	BGT4-1	BGT4-2	BGT4-3
	D	D	D	D	D	D	D	D	D	D	D	D
Cu	57.79	70.32	70.8	31.01	52.49	36.99	29.38	24.12	38.31	165.05	53.71	79.12
Zn	56.42	65.40	71.98	85.18	73.94	61.48	65.51	73.4	65.55	76.13	70.06	77.58
Ga	19.58	19.41	20.21	20.01	21.55	20.76	19.92	20.21	20.27	20.15	20.18	18.65
Rb	12.07	23.80	7.46	19.42	23.26	66.86	55.11	20.24	26	19.39	32.19	25.86
Sr	658	572	609	656	739	556	708	637	589	673	618	592
Y	9.6	10.70	11.89	13.90	14.56	16.64	9.82	11.78	11.86	12.78	14.36	15.4
Zr	38.37	46.85	49.51	93.93	90.77	62.21	62.00	75.62	73.08	83.94	94.54	97.11
Nb	1.38	2.09	1.97	2.85	2.53	2.11	1.36	1.85	1.85	1.86	2.17	2.12
Mo	0.77	0.62	0.58	–	–	–	–	0.97	1.17	1.11	0.5	0.76
Sn	0.64	0.58	0.57	–	–	–	–	0.78	0.7	0.85	0.67	0.73
Cs	0.78	0.78	0.69	2.29	1.72	2.22	2.70	1.01	1.27	0.58	0.88	1.1
Ba	252	408.00	278	530.3	486.4	301.2	322.6	479	509	428	604	492
La	5.09	7.22	7.13	10.67	9.82	8.10	8.85	8.53	8.3	8.71	9.69	11.69
Ce	11.8	16.68	16.38	21.43	20.44	17.93	18.95	19.7	18.22	21.41	22.7	27.44
Pr	1.66	2.17	2.19	3.11	3.01	2.72	2.66	2.62	2.42	2.67	3.06	3.68
Nd	8.07	10.39	10.56	12.71	12.51	12.11	11.11	11.77	11.41	12.85	14.37	16.93
Sm	1.76	2.25	2.13	2.87	2.95	2.89	2.49	2.59	2.25	2.79	3.02	3.46
Eu	0.78	0.83	0.83	0.90	0.95	0.67	0.70	0.92	0.88	1.09	1.06	0.96
Gd	1.83	2.25	2.32	2.52	2.75	2.80	2.17	2.53	2.53	2.83	3	3.26
Tb	0.29	0.33	0.38	0.40	0.44	0.45	0.32	0.36	0.36	0.44	0.46	0.48
Dy	1.74	1.97	2.28	2.45	2.62	2.91	1.87	2.29	2.19	2.37	2.73	2.81
Ho	0.39	0.40	0.46	0.51	0.53	0.6	0.36	0.46	0.44	0.49	0.52	0.53
Er	1.01	1.18	1.39	1.43	1.51	1.70	0.94	1.33	1.27	1.45	1.52	1.57
Tm	0.15	0.17	0.19	0.21	0.22	0.26	0.13	0.19	0.18	0.21	0.21	0.22
Yb	1	1.09	1.209	1.41	1.46	1.69	0.8	1.12	1.25	1.23	1.37	1.41
Lu	0.15	0.16	0.19	0.22	0.22	0.25	0.12	0.19	0.17	0.21	0.22	0.21
Hf	1.18	1.49	1.58	2.89	2.89	1.99	1.97	2.31	2.22	2.46	2.82	2.82
Ta	0.14	0.16	0.12	0.18	0.17	0.13	0.08	0.11	0.11	0.1	0.12	0.13
Pb	2.54	2.34	2.53	6.38	5.35	4.54	8.66	6.07	4.03	4.49	3.53	4.64
Bi	0.01	0.03	0.02	0.04	0.02	0.08	0.08	0.01	0.01	0.02	0.03	0.02
Th	0.94	1.42	1.37	1.78	1.88	0.28	0.53	1.61	2.44	1.48	2.01	1.96
U	0.26	0.41	0.34	0.58	0.61	0.80	0.86	0.5	0.56	0.34	0.33	0.47
LREE/HREE	4.44	5.24	4.65	5.61	5.07	4.15	6.64	5.44	5.18	5.36	5.37	6.11
ΣREE	35.78	47.16	47.69	60.91	59.50	55.14	51.52	54.65	51.94	58.79	64.01	74.72
Porphyry	V				VI			VIII		Wall-rock		
	BGT5-1	BGT5-2	BGT5-3	BGT5-4	ZK211-60	ZK211-144	ZK211-455	BGT8-700	BGT-w			
	D	QD	D	D	D	D	QD	D	T			
SiO ₂	58.95	62.05	59.98	59.92	55.68	57.72	63.89	54.87	56.96			
TiO ₂	0.82	0.69	0.88	0.83	0.88	0.88	0.64	0.81	0.52			
Al ₂ O ₃	17.88	15.73	17.76	18.07	16.92	17.01	15.46	17.88	16.08			
Fe ₂ O ₃	1.74	2.03	0.87	0.62	1.92	1.50	1.48	3.55	2.18			
FeO	1.87	3.44	1.64	1.24	4.76	4.55	2.83	3.43	5.93			
MnO	0.04	0.06	0.03	0.03	0.09	0.08	0.05	0.06	0.14			
MgO	4.35	3.91	4.41	4.81	5.01	4.51	2.91	4.35	3.37			
CaO	7.56	5.44	7.52	7.85	7.07	6.94	4.23	5.61	4.02			
Na ₂ O	4.41	4.16	4.46	4.75	3.87	4.03	4.03	4.87	3.87			
K ₂ O	0.72	0.65	0.67	0.37	1.40	1.31	2.47	1.34	3.31			
P ₂ O ₅	0.18	0.14	0.21	0.1	0.20	0.24	0.15	0.15	0.28			
LOI	1.13	1.22	1.1	0.95	1.51	0.89	1.15	2.81	2.85			
Total	99.65	99.52	99.53	99.54	99.34	99.71	99.35	99.73	99.51			
Sc	16.85	14.34	16.9	19.6	18.49	15.98	11.8	16.83	17.31			
Cr	103	146	106	92.79	77.65	91.95	51.93	63.72	52.75			
Co	9.37	17.20	6.68	5.53	27.06	20.53	16.16	23.45	17.00			
Ni	43.92	54.34	35.03	34.63	47.72	47.82	28.48	48.1	12.46			
Cu	1572	115	119.4	33.8	216	75.77	1504	193	98.01			
Zn	45.15	42.59	25.13	22.56	48.35	47.40	40.98	42.16	87.43			
Ga	21.44	18.58	19.85	19.86	19.88	19.82	19.73	21.18	19.08			
Rb	43.33	14.63	36.42	13.28	40.01	41.22	66.32	44.04	62.92			
Sr	746	559	707	748	722	739	495	840	672			
Y	15.11	14.5	15.48	17.44	13.30	14.90	19.74	10.3	18.40			
Zr	93.88	131.6	84.73	93.26	57.85	93.04	205.6	46.34	97.70			
Nb	2.48	3.2	2.69	2.69	2.76	2.96	4.55	0.77	4.10			
Mo	1.11	0.68	0.39	0.45	–	–	–	0.78	0.83			
Sn	4.88	0.78	5.87	4.15	–	–	–	0.44	0.89			
Cs	2.28	0.99	0.92	0.65	2.113	2.913	2.75	1.5	1.88			
Ba	222	354	240	221	411.8	418.9	675.5	353	809.0			
La	10.77	10.86	8.8	5.6	10.06	14.19	21.78	4.66	16.48			
Ce	29.7	22.97	28.1	16.81	21.25	29.57	44.10	11.26	36.22			
Pr	4.15	3.2	4.03	2.66	3.18	4.45	5.88	1.62	4.53			
Nd	18.63	14.95	19.22	13.84	13.15	18.25	22.88	8.42	20.58			
Sm	3.79	2.77	4.31	3.45	3.148	4.00	4.67	1.96	4.12			

(continued on next page)

Table 1 (continued)

Porphyry Sample Rock type	V				VII			Wall-rock	
	BGT5-1 D	BGT5-2 QD	BGT5-3 D	BGT5-4 D	ZK211-60 D	ZK211-144 D	ZK211-455 QD	BGT8-700 D	BGT-w T
Eu	1.21	0.92	1.27	1.14	0.98	1.18	1.05	0.82	1.34
Gd	3.36	2.87	3.78	3.53	2.71	3.39	4.01	2.01	3.98
Tb	0.53	0.39	0.55	0.55	0.41	0.49	0.61	0.33	0.61
Dy	2.91	2.5	3.09	3.16	2.42	2.84	3.59	1.93	3.23
Ho	0.57	0.49	0.59	0.62	0.49	0.56	0.72	0.38	0.68
Er	1.71	1.37	1.74	1.72	1.35	1.53	1.99	1.05	1.99
Tm	0.22	0.21	0.24	0.27	0.20	0.22	0.29	0.17	0.28
Yb	1.45	1.36	1.56	1.59	1.29	1.43	1.91	1.03	1.78
Lu	0.23	0.21	0.23	0.23	0.19	0.21	0.29	0.16	0.30
Hf	2.61	3.9	2.51	2.71	1.70	2.841	5.68	0.001	2.94
Ta	0.14	0.21	0.15	0.14	0.16	0.208	0.32	–	0.21
Pb	2.96	2.97	2.98	2.77	4.14	3.861	3.5	2.24	4.18
Bi	0.22	0.25	0.11	0.03	0.16	0.09	0.51	0.02	0.05
Th	3.29	4.09	1.94	1.58	1.22	2.614	5.38	0.48	3.82
U	1.13	1.03	0.55	0.4	0.56	1.285	1.39	0.48	1.03
LREE/HREE	6.21	5.92	5.57	3.72	5.68	6.68	7.46	4.06	9.59
ΣREE	79.28	65.13	77.58	55.23	60.90	82.38	113.8	35.85	91.96

Abbreviations: D: diorite; QD: quartz diorite; T: tuff; –: not analyzed.

including wall rock (silty tuff) and all stocks except stock VIII is represented by dominantly transitional diorites all exhibiting enrichments of LREE and large ion lithophile elements (LILE) relative to the HREE (Fig. 8a, c, e–g, j). The high-field strength element (HFSE) Nb display negative concentration anomaly. Diorite in stock VIII is different from the abovementioned samples in that it exhibits little enrichment of LREE and LILE (Fig. 8i). In agreement with the other samples it displays a negative Nb-anomaly.

4.2. Sr and Nd isotopes

Measured and initial (back-calculated to 320 Ma for the porphyries, and 330 Ma for the wall-rock tuff) isotopic ratios are reported in Table 2. Initial $^{87}\text{Sr}/^{86}\text{Sr}$ ratios range from 0.70359 to 0.70397; their initial Nd isotopes display some variations between 0.51250 and 0.51262, the ϵ_{Nd} (320 Ma) range from +2.69 to +6.34. Initial $^{87}\text{Sr}/^{86}\text{Sr}$ ratio from the tuff is slightly higher with 0.70439. The $^{143}\text{Nd}/^{144}\text{Nd}$ ratio for the tuff is 0.51249 with the ϵ_{Nd} (330 Ma) +2.74, and falls in the range of the porphyry samples. In $^{87}\text{Sr}/^{86}\text{Sr}$ vs. ϵ_{Nd} diagram (Fig. 9), all samples lie in the depleted quadrant of the Nd–Sr isotope diagram, indicating a common origin within the mantle array between depleted MORB mantle and bulk earth (e.g. Faure, 1986).

Typical adakites are characterized by ≥ 56 wt.% SiO_2 , ≥ 15 wt.% Al_2O_3 , usually < 3 wt.% MgO , low HREE (e.g., $\text{Yb} < 1.9$ ppm), high Sr, low

abundance of HFSE (e.g., $\text{Y} < 18$ ppm), and usually < 0.7045 $^{87}\text{Sr}/^{86}\text{Sr}$ (Defant and Drummond, 1990). Many samples have a chemical composition similar to that of adakitic rocks (e.g., $\text{Yb} < 1.9$ ppm, $\text{Y} < 18$ ppm, $\text{Sr} > 450$ ppm, $\text{Sr}/\text{Yb} > 20$, $^{87}\text{Sr}/^{86}\text{Sr} < 0.7045$; Tables 1, 2). Late Paleozoic adakites have been also discovered in the eastern Tianshan (Zhang et al., 2006b). In the Sr/Y vs. Y diagram (Fig. 10), some samples plot in the adakite field with the evolution of MORB and the rest samples plot in the normal arc field with the evolution of crystal fractional trend.

5. Discussion

The most important result of this study is that the ore-bearing porphyries in the Baogutu copper belt are the predominantly intermediate porphyries, formed in a transitional island arc. Magma may have been derived from the partial melting of multiple sources including oceanic crust and a subduction-modified mantle wedge, and underwent significant crystal fractionation.

5.1. Geological setting

As mentioned above, the volcanic rocks in the Darbut volcanic belt contain clear tholeiitic assemblages and a calc-alkaline assemblage,

Table 2

Rb–Sr and Sm–Nd isotopic data of representative porphyries in the Baogutu copper belt, the western Junggar.

Sample	Porphyry	Rock type	Sr (ppm)	Rb (ppm)	$^{87}\text{Rb}/^{86}\text{Sr}$	$^{87}\text{Sr}/^{86}\text{Sr}$	2om (ppm)	$I(\text{Sr})$	Sm (ppm)	Nd (ppm)	$^{147}\text{Sm}/^{144}\text{Nd}$	$^{143}\text{Nd}/^{144}\text{Nd}$	2om (ppm)	$I(\text{Nd})$	ϵ_{Nd}^t
BGT-1	I	D	25.62	938.0	0.0790	0.704052	12	0.703693	2.35	10.08	0.1409	0.512899	13	0.512586	5.08
BGT-2	II	QD	131.7	178.5	2.1361	0.713678	10	0.703971	3.85	18.87	0.1232	0.512776	11	0.512503	2.69
BGT-3-1	III	D	11.82	708.3	0.0483	0.703996	11	0.703777	1.93	8.223	0.1422	0.512886	10	0.512571	4.84
BGT-3-2	III	D	23.64	621.3	0.1101	0.704312	9	0.703811	2.28	10.00	0.1381	0.512853	12	0.512547	4.19
BGT-3-3	III	D	7.21	675.8	0.0309	0.703865	14	0.703724	2.45	10.41	0.1425	0.512862	11	0.512547	4.37
BGT-4-1	IV	D	23.12	701.2	0.0954	0.704095	11	0.703662	2.73	11.92	0.1388	0.512906	9	0.512598	5.22
BGT-4-2	IV	D	27.64	666.6	0.1199	0.704294	14	0.703749	2.63	11.66	0.1363	0.512890	14	0.512588	4.91
BGT-4-1	IV	D	18.22	685.4	0.0769	0.704184	14	0.703835	2.76	11.95	0.1400	0.512913	10	0.512603	5.37
BGT-4-2	IV	D	30.66	643.8	0.1377	0.704261	10	0.703635	3.05	13.47	0.1372	0.512902	14	0.512598	5.14
BGT-4-3	IV	D	27.06	667.0	0.1173	0.704331	10	0.703798	3.73	17.10	0.1320	0.512887	13	0.512595	4.86
BGT5-1	V	D	39.90	770.8	0.1497	0.704382	10	0.703702	3.68	17.32	0.1286	0.512859	9	0.512574	4.31
BGT5-2	V	QD	14.73	634.0	0.0672	0.704051	9	0.703746	3.21	14.14	0.1372	0.512887	10	0.512583	4.86
BGT5-3	V	D	34.16	750.4	0.1317	0.704456	13	0.703858	4.11	18.70	0.1327	0.512865	11	0.512570	4.42
BGT5-4	V	D	13.27	770.6	0.0498	0.703922	12	0.703696	3.67	13.57	0.1636	0.512947	10	0.512584	6.01
BGT8-700	VIII	D	42.42	895.5	0.1370	0.704220	12	0.703598	2.07	8.12	0.1544	0.512963	10	0.512621	6.34
BGT-w	Wall-rock	T	63.09	714.5	0.2554	0.705586	13	0.704389	4.42	20.10	0.1328	0.512784	14	0.512497	2.74

The $^{87}\text{Sr}/^{86}\text{Sr}$ ratios are normalized to $^{86}\text{Sr}/^{88}\text{Sr} = 0.1194$ and the $^{143}\text{Nd}/^{144}\text{Nd}$ ratios to $^{146}\text{Nd}/^{144}\text{Nd} = 0.7219$. Abbreviations: D: diorite; QD: quartz diorite; T: tuff. a $\epsilon_{\text{Nd}}(t) = \{[(^{143}\text{Nd}/^{144}\text{Nd})_{\text{m}} / (^{143}\text{Nd}/^{144}\text{Nd})_{\text{CHUR}}] - 1\}10^4$, using $(^{143}\text{Nd}/^{144}\text{Nd})_{\text{CHUR}} = 0.512638$. Initial (i) values calculated at 320 Ma for the porphyries, and 330 Ma for the tuff.

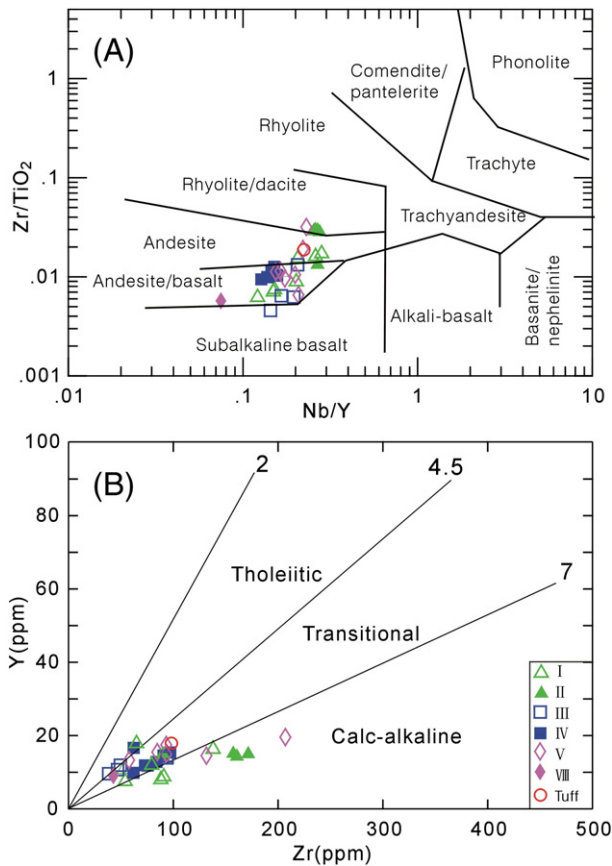


Fig. 7. (A) Zr/TiO₂ versus Nb/Y classification diagram of volcanic rocks after Winchester and Floyd (1977). (B) Zr versus Y discrimination diagram for volcanic rock affinities; almost all samples investigated in this study plot within the field of calc-alkaline, tholeiitic and transitional magmatic affinity and have a transitional character from calc-alkaline to tholeiite; ranges from Barrett and MacLean (1994).

and erupted in a transitional island arc setting from back-arc basin to island arc (Shen and Jin, 1993).

In this study, ore-bearing porphyries from the Baogutu copper belt intrude into the Darbut volcanic belt, show similar geochemistry trend but have more calc-alkaline compositions. The majority of samples are calc-alkaline and transitional intermediate igneous rocks (Fig. 7) and have distinct fractionated REE patterns (Fig. 8). In Fig. 11, the data are plotted on a tectonic discrimination diagram for the ore-bearing porphyries and their wall rocks. All samples have low Nb concentrations relative to La and Y and are therefore similar to island arc rocks. Most samples plot close to the La-apex showing an affinity to calc-alkaline island arc basalts. Those samples plotting towards the Y-apex reveal an affinity with island arc tholeiites. Calc-alkaline rocks are typical constituents of mature island arcs, whereas tholeiitic rocks may be associated with emerging island arcs (e.g. Kuno, 1966; Miyashiro, 1974), mid-ocean ridges, and backarc-basin spreading centers (e.g. Gill, 1976). We therefore further suggest that the ore-bearing diorite porphyries formed in an island arc setting, with transitional features from immature arc or backarc-basin to mature arc. This arc is likely a segment of the Darbut transitional island arc between the Siberian and Tarim plates.

5.2. Petrogenesis

The ore-bearing porphyries in the Baogutu copper belt have distinct fractionated REE patterns (Fig. 8). The calc-alkaline quartz diorites (Fig. 8b, d, h) exhibit strongly fractionated REE patterns and low HREE abundances due to fractionation of hornblende, which plays an important role in thick and mature island arcs (e.g., Green, 1980;

Kay, 1984). The LREE abundances increase with the degree of differentiation, e.g. the quartz diorite (ZK702-190) shows the highest enrichment in LREE (Fig. 8b), suggesting that the sample is probably related by crystal fractionation. This is supported by the transitional distribution of most samples plot between the partial melting line and the fractional crystallization line in the La/Yb vs. La diagram (Fig. 12). The dominant transitional diorites show fractionated REE patterns and enrichments of LILE with a negative Nb anomaly (Fig. 8). These chemical characteristics support melting of a subduction-modified mantle comprising fluids and melts from a dehydrating slab (e.g., Kay, 1984; Münker et al., 2004).

One sample exhibits little enrichment of LREE and LILE and a negative Nb anomaly (Fig. 8i). The trace element pattern is similar to that of basalt from incipient and immature island arcs (e.g. Stern et al., 2003). Such low enrichment of the LREE suggests a very small amount of a recycled sedimentary component in this sample.

Geochemical evidence discussed above is supported by the isotopic data. When all isotopic data are examined together, the initial ⁸⁷Sr/⁸⁶Sr ratios of the ore-bearing porphyries range from 0.70359 to 0.70397, similar to those of the typical island arc lavas (White and Patchet, 1984). The ¹⁴³Nd/¹⁴⁴Nd ratios range from 0.51250 and 0.51262, being lower than typical island arc lavas (0.51297–0.51305, White and Patchet, 1984). The εNd values range from 2.7 to 6.3 (Table 2) and indicate, together with the individual initial ⁸⁷Sr/⁸⁶Sr values as shown in Fig. 10, a common origin within the mantle array between depleted MORB mantle and bulk earth (e.g. Faure, 1986). Most porphyry samples show high and similar initial εNd-values of +4 to +6 (Table 2), supporting a comagmatic origin and representing a MORB-like mantle. A porphyry sample in stock II has lower initial εNd-value of +2.7, inferring a juvenile crustal component of the Darbut transitional island arc. A tuff sample with a silty component also yields a low initial εNd-value of +2.7, suggesting the involvement of terrigenous material.

Based on geochemical characteristics, we infer that the ore-bearing porphyry stocks in the Baogutu copper belt were most likely derived by partial melting of multiple sources including a subduction-modified mantle wedge and the subducting early Carboniferous oceanic crust. Melts underwent significant crystal fractionation during convergence between the paleo-Junggar ocean and the Darbut arc.

5.3. Ore-forming conditions

Based on previous work, metallogeny show that the basaltic oceanic crust has high abundance of metals (Cu, Au), and adakitic magmas may contain the dominant volatile components (Kay and Mpodozis, 2001; Defant et al., 2002; Mungall, 2002; Richards and Kerrich, 2007). The result of a early Carboniferous Junggar basaltic oceanic crust subduction process, large-scale decomposition of hornblende in subducting crust released large amounts of volatile components and Cu and Au metals into the overlying mantle wedge, causing the formation of intermediate dioritic magma. When the dioritic magma ascends from the mantle wedge, the pressure rapidly decreases, the magmas release Cu, Au, and volatiles leading to the formation of ore-forming fluids.

To allow Cu and Au enrichment in the magma, the process of magma generation in subduction-modified mantle wedge and subsequent fluid release from the magma, requires high oxygen fugacity, which will also restrain the stability of sulfides (Silltoe, 1997; Metrich et al., 1999; Audetat et al., 2004). Our petrographic results show the diorite porphyries in the Baogutu copper belt formed at high oxygen fugacity, with hydrothermal magnetites widespread in the potassic alteration zone (Fig. 6D) and significant amounts of gypsum veins observed in thin sections of the rocks and outcrops in stock V. Analyses show that biotite in the diorite porphyries is magnesium-rich with Mg/(Mg + Fe + Mn) values of 0.60 (Shen and Jin, 1993).

Widespread micro-fissures and intense alteration are very important during the formation of an ore body. We recognize the breccias in

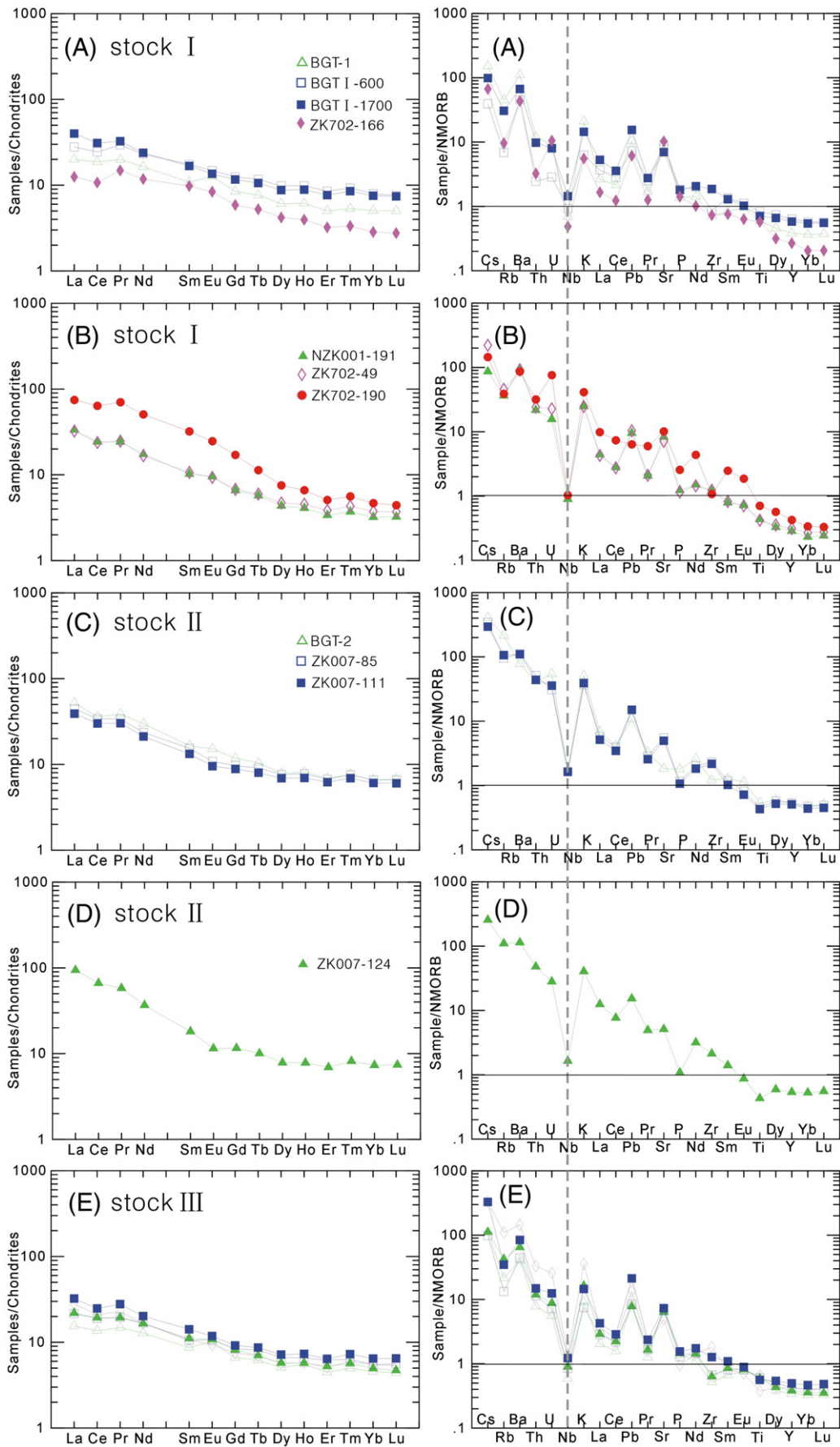


Fig. 8. Chondrite normalized (Nakamura, 1974) REE distribution and patterns of trace elements normalized (Sun and McDonough, 1989) to N-MORB for the ore-bearing porphyries and tuff in the Baogutu copper belt.

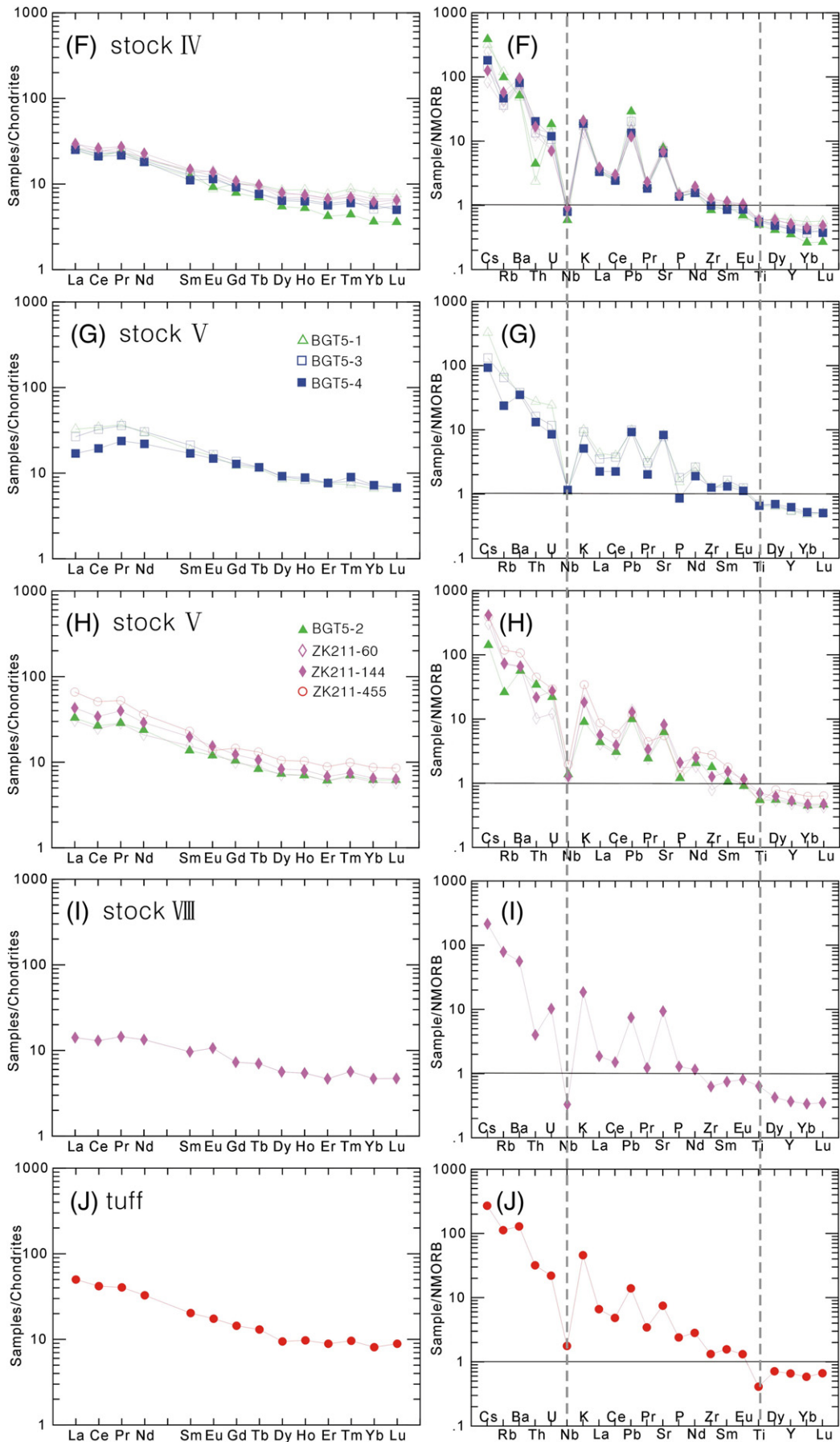


Fig. 8 (continued).

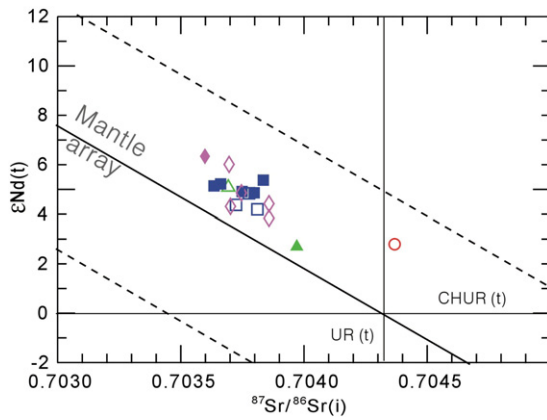


Fig. 9. $\epsilon\text{Nd}(t)$ versus initial $^{87}\text{Sr}/^{86}\text{Sr}$ diagram indicating initial (320 Ma for ore-bearing porphyries and 330 Ma for tuff) isotope characteristics of the ore-bearing porphyries and tuff samples in the Baogutu copper belt. Symbols are the same as in Fig. 7.

stock V and surrounding wall-rocks, and numerous quartz–sulfide veinlets fill micro-fissures in the breccias where the copper ore bodies concentrate. All rocks in the ore-bearing porphyry study area were subjected to intense hydrothermal alteration. A typical diorite-type porphyry copper model in stock V deposit has been recognized, with a large porphyry copper deposit occurring in the potassic alteration zone, and further overprinted by the phyllic alteration. About twenty $\delta^{34}\text{S}$ composition of sulfides in the Baogutu stock V deposit range from 0.4‰ to 1.0‰ and are very close to that of mantle sulfur (Shen and Jin, 1993), indicating a deep sulfur source.

The diorite porphyries are associated with copper mineralization. The main copper ore bodies are hosted and accompanied by hydrothermal alteration of the porphyries. We suggest that the occurrence of diorites can be used as potential prospecting targets in the western Junggar.

6. Conclusions

The Baogutu copper belt, which occurred in the Darbut transitional island arc between the Siberian and Tarim plates, is the second largest porphyry copper belt in NW China. This work is the first attempt to elucidate the petrology and petrogenesis of the ore-bearing porphyry stocks in the Baogutu copper belt by combining chemical data with radiogenic (Sr and Nd) isotopes of the six ore-bearing diorite porphyry stocks in the Baogutu copper belt.

The ore-bearing porphyries in the Baogutu copper belt are dioritic porphyritic stocks rather than granodiorite stocks as previously

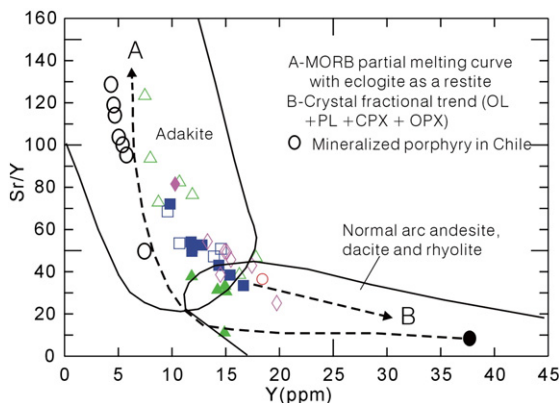


Fig. 10. Diagram of Sr/Y vs. Y (Defant and Drummond, 1993). Symbols are the same as in Fig. 7. The data on mineralized porphyries in Chile are from Oyarzún et al. (2001).

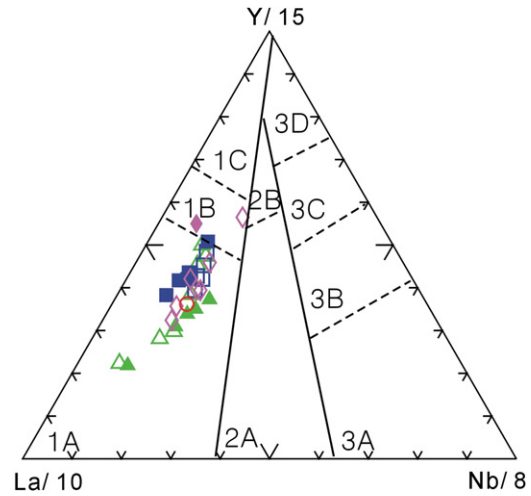


Fig. 11. Tectonic discrimination diagram based on immobile trace elements for ore-bearing porphyries and tuff from the Baogutu copper belt (after Cabanis and Lecolle, 1989; also in Rollinson, 1993). Explanation: 1A = calcalkaline basalts, 1C = volcanic-arc tholeiites, 1B = overlap area between 1A and 1C; 2A = continental basalts, 2B = backarc-basin basalts; 3A = alkali basalts; 3B, C = enriched MORB; 3D = depleted MORB. Symbols are the same as in Fig. 7.

identified. The dioritic porphyritic stocks consist mainly of diorite/quartz diorite, diorite porphyry/quartz diorite porphyry, related breccias, and minor granodiorite porphyry. The copper mineralization is mainly hosted in the dioritic porphyritic stocks and related breccias.

The ore-bearing porphyries are predominantly intermediate in composition and have a transitional character from calc-alkaline to tholeiite with distinct enrichment in LREE and LILE and depletion in the Nb and the HREE. These rocks also show positive $\epsilon\text{Nd}(t)$ values (+2.7 to +6.3) and low initial $^{87}\text{Sr}/^{86}\text{Sr}$ values of 0.70359–0.70397. These data suggest that the ore-bearing porphyries may be derived from the partial melting of multiple sources including components of oceanic crust (e. g. subducted sediment) and a subduction-modified mantle wedge, and underwent significant crystal fractionation during convergence between the paleo-Junggar ocean and the Darbut arc.

The copper porphyry systems in the Baogutu copper belt must have had relatively high oxygen fugacities, together with widespread micro-fissures and intense alteration, allowing the deposits to develop. Diorite porphyry is associated with copper mineralization and thus can be considered as a new exploration target applicable to the search for new porphyry copper deposits in the western Junggar.

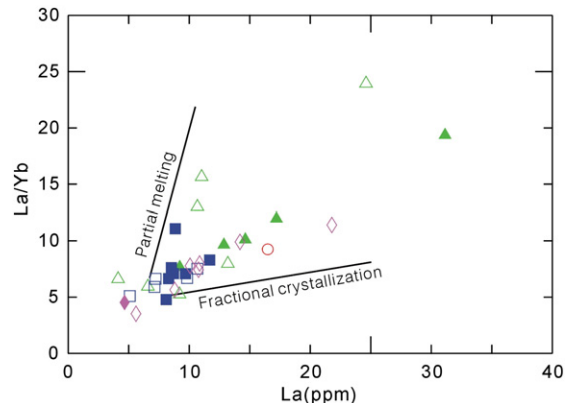


Fig. 12. Diagram of La/Yb vs. La for the diorite porphyries and tuff from the Baogutu copper belt. Symbols are the same as in Fig. 7.

Acknowledgements

This paper was financially supported by the Innovative Project of the Chinese Academy of Sciences (Grant No. KZCX2-YW-107), and 305 Project of the State Science and technology Program of China (Grant No. 2006BAB07B01-01). Thanks are given to Prof. Jingbing Wang and Rui Zhang for thoughtful discussions and for providing relevant references. In particular, we express our gratitude to Editor Prof. Wenjiao Xiao and two anonymous reviewers for their critical reviews and outstanding job on improvement of the manuscript.

References

- Audetat, T., Pettke, D., Dolejs, 2004. Magmatic anhydrite and calcite in the ore-forming quartz-monzodiorite magma at Santa Rita, New Mexico (USA): genetic constraints on porphyry-Cu mineralization. *Lithos* 72, 147–161.
- Barrett, T.J., MacLean, W.H., 1994. Chemostratigraphy and hydrothermal alteration in exploration for VHMS deposits in greenstones and younger volcanic rocks. In: Lentz, D.R. (Ed.), *Alteration and Alteration Processes Associated with Ore-Forming Systems*. Short Course Notes, vol. 11. Geological Association of Canada, pp. 433–467.
- Barthelmy, D.A., 1979. Regional geology of El Arco porphyry copper deposit, Baja California. In: Abbott, P.L., Gastil, R.G. (Eds.), *Baja California geology*. San Diego State University, CA, pp. 127–138.
- Buslov, M.M., Fujiwara, Y., Iwata, K., Semakov, N.N., 2004. Late Paleozoic–Early Mesozoic geodynamics of Central Asia. *Gondwana Research* 7, 791–808.
- Cabanis, B., Lecolle, M., 1989. Le diagramme La/10–Y/15–Nb/8: un outil pour la discrimination des séries volcaniques et la mise en évidence des processus de mélange et/ou de contamination crustale. *Comptes Rendus de l'Académie des Sciences. Serie 2* 309, 2023–2029.
- Chai, F., Mao, J., Dong, L., Yang, F., Liu, F., Geng, X., Zhang, Z., 2009. Geochronology of metarhyolites from the Kangbutiebao formation in the Kelang basin, Altay Mountains, Xinjiang: implications for the tectonic evolution and metallogeny. *Gondwana Research* 16, 189–200 (this issue).
- Chen, B., Jahn, B.-M., 2004. Genesis of post-collisional granitoids and basement nature of the Junggar Terrane, NW China: Nd–Sr isotope and trace element evidence. *Journal of Asian Earth Sciences* 23, 691–703.
- Chen, B., Arakawa, Y., 2005. Elemental and Nd–Sr isotopic geochemistry of granitoids from the West Junggar foldbelt (NW China), with implications for Phanerozoic continental growth. *Geochimica et Cosmochimica Acta* 69, 1307–1320.
- Chen, F., Satir, M., Ji, J., Zhong, D., 2002. Nd–Sr–Pb isotopic composition of the Cenozoic volcanic rocks from western Yunnan, China: evidence for enriched mantle source. *Journal of Asian Earth Sciences* 21, 39–45.
- Cheng, Y., Zhang, R., 2006. Mineralization regularity of Cu–Au deposits in the Baogutu area, western Junggar, Xinjiang. *Geology and Prospecting* 42, 11–15 (in Chinese with English abstract).
- Defant, M.J., Drummond, M.S., 1990. Derivation of some modern arc magmas by melting of young subduction lithosphere. *Nature* 347, 662–665.
- Defant, M.J., Drummond, M.S., 1993. Mount St. Helens: potential example of the partial melting of the subducted lithosphere in a volcanic arc. *Geology* 21, 547–550.
- Defant, M.J., Xu, J.F., Kepezhinskis, P., Wang, Q., Zhang, Q., Xiao, L., 2002. Adakites: some variations on a theme. *Acta Petrologica Sinica* 18, 129–142.
- Faure, G., 1986. *Principles of Isotope Geology*, 2nd ed. Wiley, New York.
- Gill, J.B., 1976. Composition and age of Lau Basin and ridge volcanic rocks: implications for evolution of an interarc basin and remnant arc. *Geological Society of America Bulletin* 87, 1384–1395.
- Green, T.H., 1980. Island arc and continental building magmatism – a review of petrogenetic models based on experimental petrology and geochemistry. *Tectonophysics* 63, 367–385.
- Han, B.F., Ji, J.Q., Song, B., Chen, L.H., Zhang, L., 2006. Late Paleozoic vertical growth of continental crust around the Junggar Basin, Xinjiang, China (Part II): timing of post-collisional plutonism. *Acta Petrologica Sinica* 22, 1077–1086 (in Chinese with English abstract).
- Hollister, V.F., Potter, R.R., Barker, A.L., 1974. Porphyry-type deposits of Appalachian Orogen. *Economic Geology* 69, 618–630.
- Hu, A.Q., Wang, Z.G., Tu, G.C., 1997. Geological Evolution and Diagenesis and Metallogenesis in Northern Xinjiang, China. Science Press, Beijing, 1–213 pp. (in Chinese with English abstract).
- Jahn, B.M., Wu, F.Y., Chen, B., 2000. Massive granitoid generation in central Asia: Nd isotopic evidence and implication for continental growth in the Phanerozoic. *Episodes* 23, 82–92.
- Kay, R.W., 1984. Elemental abundances relevant for identification of magma sources. *Philosophical Transactions of the Royal Society of London. A* 310, 535–547.
- Kay, S.M., Mpodozis, C., 2001. Central Andean ore deposits linked to evolving shallow subduction systems and thickening crust. *GSA Today* 11, 4–9.
- Kuno, H., 1966. Lateral variation of basalt magma types across continental margins and island arcs. *Bulletin of Volcanology* 29, 195–222.
- Li, H.Q., Chen, F.W., 2004. Isotopic geochronology of regional mineralization in Xinjiang, China. Geological publishing house, Beijing, 19–42 pp. (in Chinese with English abstract).
- Lowell, J.D., Guilber, T.J.M., 1970. Lateral and vertical alteration mineralization zoning in porphyry ore deposits. *Economic Geology* 65, 373–404.
- Martins, G., Oliveira, E.P., Lafon, J.-M., 2009. The Algodões amphibolite–tonalite gneiss sequence, Borborema Province, NE Brazil: Geochemical and geochronological evidence for Palaeoproterozoic accretion of oceanic plateau/back-arc basalts and adakitic plutons. *Gondwana Research* 15, 71–85.
- Metrich, N., Schiano, P., Clacchiatti, R., Maury, R.C., 1999. Transfer of sulfur in subduction settings: an example from Batan Island (Luzon volcanic arc, Philippines). *Earth and Planetary Science Letters* 167, 1–14.
- Miyashiro, A., 1974. Volcanic rock series in island arcs and active continental margins. *American Journal of Science* 274, 321–355.
- Mungall, J.E., 2002. Roasting the mantle: slab melting and the genesis of major Au and Au-rich Cu deposits. *Geology* 30, 915–918.
- Münker, C., Wörner, G., Yogodzinski, G., Churikova, T., 2004. Behaviour of high field strength elements in subduction zones: constraints from Kamchatka–Aleutian arc lavas. *Earth and Planetary Science Letters* 224, 275–293.
- Nakamura, N., 1974. Determination of REE, Ba, Mg, Na and K in carbonaceous and ordinary chondrites. *Geochimica et Cosmochimica Acta* 38, 757–773.
- Oyarzún, R., Márquez, A., Lillo, J., López, I., Rivera, S., 2001. Giant versus small porphyry copper deposits of Cenozoic age in northern Chile: adakitic versus normal calc-alkaline magmatism. *Mineralium Deposita* 36, 794–798.
- Qin, K.Z., Sun, S., Fang, T.H., Wang, S.L., Liu, W., 2002. Paleozoic epithermal Au and porphyry Cu deposits in North Xinjiang, China: epochs, features, tectonic linkage and exploration significance. *Resource Geology* 52, 291–300.
- Richards, J.P., Kerrich, R., 2007. Special paper: adakite-like rocks: their diverse origins and questionable role in metallogenesis. *Economic Geology* 102, 537–576.
- Rollinson, H., 1993. *Using geochemical data: evaluation, presentation, interpretation*. Prentice Hall, Longman Scientific and Technical, Harlow, United Kingdom (GBR) 352.
- Safonova, I.Y., Buslov, M.M., Iwata, K., Kokh, D.A., 2002. Fragments of Vendian–Early Carboniferous oceanic crust of the Paleo-Asian Ocean in foldbelts of the Altai–Sayan region of Central Asia: geochemistry, biostratigraphy and structural setting. *Gondwana Research* 7, 771–790.
- Shen, Y.C., Jin, C.W. (Eds.), 1993. *Magmatism and Gold Mineralization in Western Junggar*. Beijing Science Press, pp. 113–172 (in Chinese with English abstract).
- Shen, Y.C., Jin, C.W., Qi, J.Y., 1993. Ore-forming model and mechanism of gold mineralization area in west Junggar. In: Tu Guangchi (Ed.), *New developments of Solid Earth Sciences of Northern Xinjiang*. Science Press, Beijing, pp. 137–150 (in Chinese).
- Shen, Y.C., Xiao, Z., Liu, H., 1996. The characteristics of the Altai–Junggar gold mineralization belt. In: Jin, C. (Ed.), *Geology of Main Gold Metallogenic Belts in Northern Part of China*. Seismological Press, Beijing, pp. 7–31 (in Chinese with English abstract).
- Shen, P., Shen, Y.C., Liu, T.B., Lu, J.J., Wei, J.P., Song, G.X., Meng, L., 2008. Late Paleozoic gold and copper mineralization and tectonic evolution in Northwestern Xinjiang, China. *Acta Petrologica Sinica* 24, 1087–1100 (in Chinese with English abstract).
- Sillitoe, R.H., 1997. Characteristics and controls of the largest porphyry copper–gold and epithermal gold deposits in the circum-Pacific region. *Australian Journal of Earth Sciences* 44, 373–388.
- Song, H.X., Liu, Y.L., Qu, W.J., Song, B., Zhang, R., Cheng, Y., 2007. Geological characters of Baogutu porphyry copper deposit in Xinjiang, NW China. *Acta Petrologica Sinica* 23, 1891–1988 (in Chinese with English abstract).
- Stern, R.J., Fouch, M.J., Klempner, S., 2003. An overview of the Izu–Bonin–Mariana Subduction Factory. *AGU Geophysical Monograph* 138, 175–222.
- Su, Y.P., Tang, H.F., Hou, G.S., 2006. Geochemistry of aluminous A-type granites along Darabut tectonic belt in West Junggar, Xinjiang. *Geochimica* 35, 1–5 (in Chinese with English abstract).
- Sun, S.S., McDonough, W.F., 1989. Chemical and isotopic systematics of oceanic basalts: implications for mantle composition and processes. In: Saunders, A.D., Norry, M.J. (Eds.), *Magmatism in Ocean Basins*. Special Publication. Geological Society of London, pp. 313–345.
- Titley, S.R., Beane, R.E., 1981. Porphyry copper deposits: part I, geologic settings, petrology and tectogenesis. In: Skinner, B.J. (Ed.), *Economic geology 75th anniversary volume; 1905–1980*. Society of Economic Geologists Publication, pp. 214–235.
- Wang, J.B., Xu, X., 2006. Postcollisional tectonic evolution and metallogenesis in Northern Xinjiang, China. *Acta Geologica Sinica* 80, 23–31 (in Chinese with English abstract).
- Wang, R., Zhu, Y.F., 2007. Geology of the Baobei gold deposit in Western Junggar and Zircon SHRIMP age of its wall-rocks, Western Junggar (Xinjiang, NW China). *Geological Journal of China Universities* 13, 590–602.
- White, W.M., Patchet, P.J., 1984. Hf–Nd–Sr isotopes and incompatible element abundances in island arcs: implications for magma origins and crust–mantle evolution. *Earth and Planetary Science Letters* 67, 167–185.
- Winchester, J.A., Floyd, P.A., 1977. Geochemical discrimination of different magma series and their differentiation products using immobile elements. *Chemical Geology* 20, 325–343.
- Xiao, W.J., Windley, B.F., Fang, A.M., Zhou, H., Yuan, C., Wang, Z.H., Hao, J., Hou, Q.L., Li, J.L., 2001. Paleozoic–Early Mesozoic accretionary tectonics of the western Kunlun Range, NW China. *Gondwana Research* 4, 826–827.
- Xiao, W.J., Windley, B.F., Badarch, G., Sun, S., Li, J., Qin, K.Z., Wang, Z.H., 2004. Paleozoic accretionary and convergent tectonics of the southern Altai: implications for the lateral growth of Central Asia. *Journal of the Geological Society (London)* 161, 339–342.
- Xiao, W.J., Han, C.M., Yuan, C., Sun, M., Shoufa, L., Chen, H.L., Li, Z.L., Li, J.L., Sun, S., 2008. Middle Cambrian to Permian subduction-related accretionary orogenesis of Northern Xinjiang, NW China: implications for the tectonic evolution of central Asia. *Journal of Asian Earth Sciences* 32, 102–117.

- Zhang, R., Zhang, Y.X., Dong, G.S., 2005. Geological characteristics and origin of Baogutou copper deposit in Xinjiang. 2005 meeting of Chinese Science and technology Association, Ürümqi, pp. 1–6 (in Chinese).
- Zhang, L.C., Wan, B., Jiao, X.I., Zhang, R., 2006a. Characteristics and geological significance of adakitic rocks in copper-bearing porphyry in Baogutu, western Junggar. *Geology in China* 33 (3), 626–631 (in Chinese with English abstract).
- Zhang, L.C., Xiao, W.J., Qin, K.Z., Zhang, Q., 2006b. The adakite connection of the Tuwu-Yandong copper porphyry belt, eastern Tianshan, NW China: trace element and Sr–Nd–Pb isotope geochemistry. *Mineralium Deposita* 41, 188–200.
- Zhang, R., Zhang, Y.X., Dong, G.S., Wang, J., Li, L.Q., 2006c. Major breakthrough in copper exploration in the Baogutu porphyry copper deposit, western Junggar, Xinjiang, and its significance. *Geology in China* 33, 1354–1360 (in Chinese with English abstract).
- Zhang, Z., Zhou, G., Kusky, T.M., Yan, S., Chen, B., Zhao, L., 2009. Late Paleozoic volcanic record of the Eastern Junggar Terrane, Xinjiang, Northwestern China: major and trace element characteristics, Sr–Nd isotopic systematics and implications for tectonic evolution. *Gondwana Research* 16, 201–215 (this issue).
- Zhao, Z., Xiong, X., Wang, Q., Bai, Z., Qiao, Y., 2009. Late Paleozoic underplating in North Xinjiang. *Gondwana Research* 16, 216–226 (this issue).